

7

Prism Design and Applications

Paul R. Yoder, Jr.

CONTENTS

7.1	Introduction and Summary	388
7.2	Geometric Relationships.....	389
7.2.1	Refraction and Reflection at Air–Glass Interfaces	389
7.2.2	Beam Displacements Caused by Plane-Parallel Plates.....	390
7.2.3	Tunnel Diagrams for Prisms	391
7.2.4	Total Internal Reflection.....	396
7.2.5	Aberrations Caused by Prisms and Plates.....	400
7.3	Beam-Folding Prisms	401
7.3.1	Right-Angle Prism	401
7.3.2	Beam Splitter (or Beam Combiner) Cube Prism	402
7.3.3	Rhomboid Prism	403
7.3.4	Porro Prism	404
7.3.5	Abbe–Porro Prism.....	405
7.3.6	Amici Prism.....	406
7.3.7	Frankford Arsenal Type 1 and Type 2 Prisms.....	408
7.3.8	Penta Prism.....	408
7.3.9	Roof Penta Prism.....	409
7.3.10	45° Bauernfeind Prism	410
7.4	Image Erecting Prisms	411
7.4.1	Porro Erecting System.....	412
7.4.2	Abbe–Porro Erecting System	414
7.4.3	Abbe–Koenig Prism.....	416
7.4.4	Roof Schmidt Prism.....	418
7.4.5	Leman Prism	419
7.4.6	Amici/Penta and Right-Angle/Roof Penta Erecting Systems.....	421
7.4.7	60° Prism/Roof Prism System.....	421
7.5	Image-Rotating Prisms.....	422
7.5.1	Dove Prism.....	422
7.5.2	Double-Dove Prism	423
7.5.3	Reversion Prism	426
7.5.4	Pechan Prism	426
7.5.5	Delta Prism	429
7.6	Other Prism Types	432
7.6.1	Internally Reflecting Axicon Prism.....	432
7.6.2	Cube-Corner Prism.....	433

7.6.3	Ocular Prism for a Coincidence Range Finder	436
7.6.4	Biocular Prism System	438
7.6.5	Dispersing Prisms.....	439
7.6.6	Thin Wedge Prisms	441
7.6.6.1	Thin Wedge.....	441
7.6.6.2	Risley Wedge System.....	442
7.6.6.3	Image-Deviating Sliding Wedge.....	443
7.6.6.4	Focus-Adjusting Wedge System.....	444
7.7	Anamorphic Prism Systems.....	446
	References.....	447

7.1 Introduction and Summary

In this chapter, we first address the geometric relationships that govern the function of prisms and then consider specific designs for prisms that serve useful purposes in optical instruments, but do not contribute optical power and, hence, cannot form images by themselves. Small motions or misalignments of some such components relative to other system components may not affect overall system performance. Examples are a Porro prism that tilts about an axis perpendicular to the plane of reflection and a cube-corner prism that tilts about any of three orthogonal axes. In both cases, for small tilts of the optic, the reflected beams are not disturbed. Prisms with this characteristic are called constant-deviation prisms with respect to those particular axes.

In spite of these and other unique capabilities of specific prism types, it is good engineering practice to carefully establish and maintain the locations and orientations of all prisms. Mountings for these components then are opto-mechanical design tasks. They are considered in Chapter 8 of this Volume.

The principal uses of prisms in optical instruments are as follows:

- To bend (deviate) light around corners
- To fold an optical system into a given shape or package size
- To provide proper image orientation
- To displace the optical axis laterally
- To adjust optical path length
- To divide or combine beams by intensity sharing or aperture sharing at a pupil
- To divide or combine images at an image plane
- To provide dynamic scanning of beams
- To disperse light spectrally
- To modify the aberration balance of the system of which they are a part

Designs for prisms that accomplish selected functions from this list are described in this chapter. Equations for the key parameters listed in Table 7.1 are provided for most prism configurations. The numerical results of applying each equation for an assumed value of prism aperture A (typically 38.100 mm [1.500 in.]) are included as worked-out design examples.

TABLE 7.1

Definitions of Parameters Used in Prism Designs

Parameter	Definition
A	Aperture diameter required for passage of collimated beam
B, C, D , etc.	Other linear dimensions
a, b, c, d , etc.	Typical bevel or other dimensions
$\alpha, \beta, \gamma, \delta, \theta, \phi$, etc.	Angles
ρ	Glass density
t_A	Axial path length
V	Prism volume (neglecting bevels and to sharp corners)
W	Prism weight
N	Glass refractive index

Note: As discussed in Chapter 11 of this Volume, the stresses created by temperature changes may determine upper limits on bond sizes.

A reference commonly used by optical designers and engineers as a guide in designing prisms is Volume II, Chapter 3 of MIL-HDBK-141, *Optical Design*, published by the U.S. Department of Defense in 1962. That chapter gives generic equations for prism dimensions, axial path lengths, and tunnel diagrams for many common types of prisms. Most examples included there were previously described in a now out-of-print book, *Design of Fire Control Optics*, ORDM 2-1, written by Otto K. Kaspereit at the U.S. Army's Frankford Arsenal and published in 1953. Excerpts from one or both of these references were published by Walles and Hopkins (1964), Hopkins (1965), De Vany (1981), Wolfe (1995), Smith (2008), and Yoder (2008), as well as in earlier editions of the present work. To make this design information readily available, we here summarize the designs for 31 types of prisms and prism subassemblies. All types are represented by geometric or functional diagrams. These are not always to exact scale. Dimensional equations based on a prism aperture of $A \times A$ are given for most types. In some cases, isometric views and equations for approximate prism volume and weight are provided. This information would be needed to utilize the mounting techniques described in Chapter 8 of this Volume.

7.2 Geometric Relationships

7.2.1 Refraction and Reflection at Air–Glass Interfaces

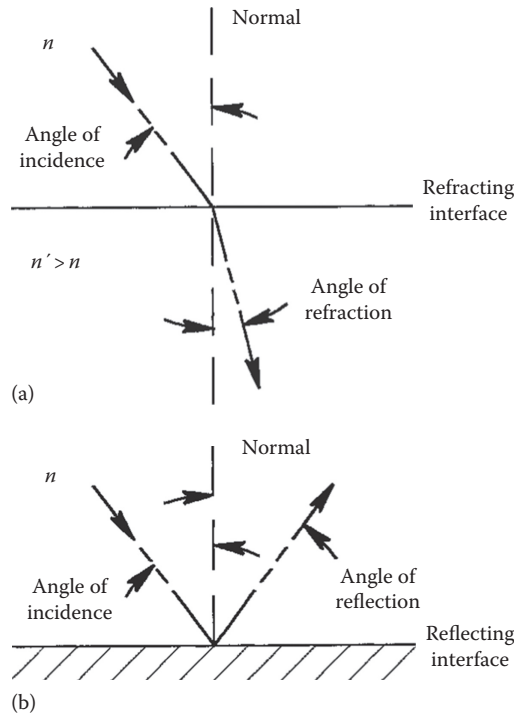
The behavior of light rays at an interface between two media such as air and glass is determined by the laws of refraction and reflection (see Figure 7.1). Refraction is expressed by Snell's law, which is written as follows:

$$n_i \sin I_i = n'_i \sin I'_i \quad (7.1)$$

where

n_i and n'_i are the refractive indices before and after the i th interface

I_i and I'_i are the angles of incidence and refraction of a given ray relative to the surface normal before and after the interface, respectively

**FIGURE 7.1**

(a) Refraction and (b) reflection at a flat interface.

Reflection at an optical surface follows the law of reflection, which is

$$I' = -I \quad (7.2)$$

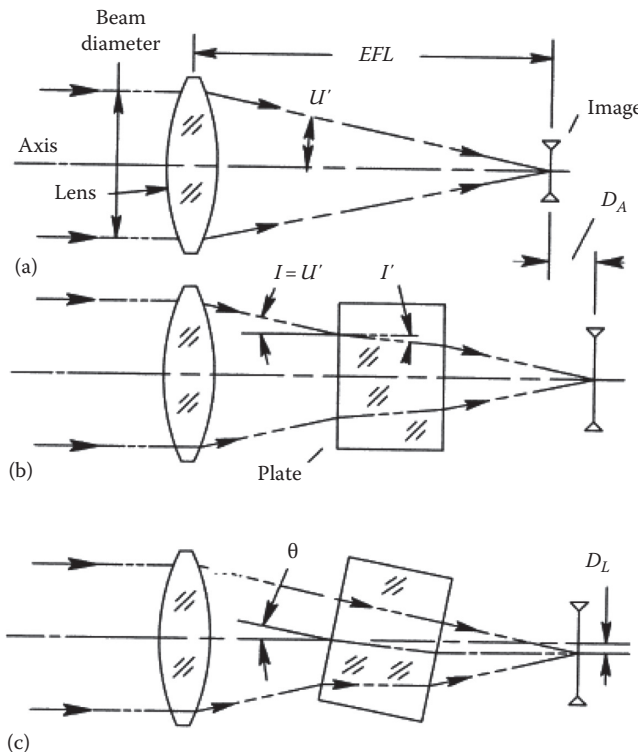
The angles are those of incidence (I) and reflection (I') at the interface. The negative algebraic sign indicates that the incident and reflected rays lie on opposite sides of the surface normal at the point of incidence.

7.2.2 Beam Displacements Caused by Plane-Parallel Plates

The refraction-induced axial displacement of an image formed through a plane-parallel plate of index n and thickness t_A oriented normal to the axis is illustrated by Figure 7.2. View (a) shows the lens and the image of a distant object without the plate. In view (b), the plate is inserted at a selected location along the axis. Neither the effective focal length (EFL) of the lens nor the size of the image is affected by insertion of the plate. The optical axis is not deviated. The image is translated axially in the direction away from the lens by a distance D_A , given paraxially* by

$$D_A = \frac{(n-1)t_A}{n} \quad (7.3)$$

* Small-angle approximation.

**FIGURE 7.2**

(a) Simple optical system comprising an objective lens focusing a beam from an infinitely distant object to its image. (b) Axial shift D_A of the image by a plane-parallel glass plate or prism with refracting surfaces oriented perpendicular to the axis of a convergent beam. (c) Lateral displacement D_L of the image by a tilted plane-parallel plate or prism.

If the same plate is tilted with respect to the axis by an angle θ , both the axis and the image are translated laterally by D_L (see Figure 7.2b). This displacement is given exactly as

$$D_L = t_A \sin \theta \left[1 - \left(\frac{1 - \sin^2 \theta}{n^2 - \sin^2 \theta} \right)^{1/2} \right] \quad (7.4)$$

or, paraxially, by

$$D_L = t_A \arccos \theta \left(\frac{n-1}{n} \right) \quad (7.5)$$

where θ is the plate's tilt angle in radians. We illustrate the use of these equations in the following Design Example 7.1.

7.2.3 Tunnel Diagrams for Prisms

Reflection at a mirror or within a prism constitutes a form of *folding* of the ray paths. In Figure 7.3, a lens images a distant vertical arrow (not shown) as the image $A'B'$ by way of the mirror indicated by the dashed line MM' . Note that if the page were to be folded

DESIGN EXAMPLE 7.1 AXIAL AND LATERAL SHIFTS OF THE IMAGE DUE TO INSERTION OF A PLANE-PARALLEL PLATE

A 25.400 mm (1.000 in.) diameter collimated beam enters a positive lens of focal length 125.000 mm (4.921 in.) and aperture 30.000 mm (1.181 in.). A 25.000 mm (0.984 in.) thick glass plane-parallel plate with index $n = 1.517$ is inserted perpendicularly to the axis into the converging beam from the lens. (a) How much is the image shifted axially? (b) If the plate described in (a) is tilted by $\theta = 20^\circ$, how much are the axis and the image displaced laterally? (c) Recalculate D_L paraxially and compare that result to that of (b):

- (a) From Equation 7.3, $D_A = (1.517 - 1)(25.000)/1.517 = 8.520 \text{ mm (0.335 in.)}$
- (b) Exactly from Equation 7.4,

$$\begin{aligned} D_L &= [25.000 \times 0.342] \{1 - [(1 - 0.3422)/(1.5172 - 0.3422)]^{1/2}\} \\ &= [8.550] [1 - (1 - 0.342)^{1/2}] = 17.678 \times 0.473 = 3.114 \text{ mm (0.123 in.)} \end{aligned}$$

- (c) Paraxially, from Equation 7.5,

$$\begin{aligned} D_L &= (25.000)(20.000/57.296)(0.517/1.517) \\ &= 2.974 \text{ mm (0.117 in.)} \end{aligned}$$

The agreement error between the exact result in (b) and the paraxial result in (c) is 4.5%.

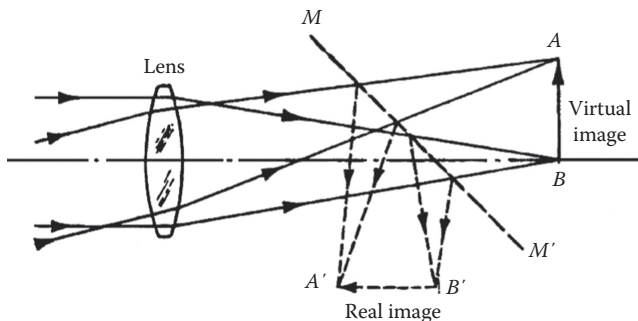


FIGURE 7.3
Folding an optical path with a mirror.

along the line MM' , the virtual image AB^* and the solid-line rays would exactly coincide with the real image $A'B'$ and the reflected (dashed line) rays. It is frequently convenient to represent such a folded diagram by its simpler in-line or unfolded counterpart. With internally reflecting prisms, an unfolded diagram is called a tunnel diagram. Such diagrams are particularly helpful when designing an optical instrument using prisms, because they facilitate the approximate determination of required apertures and, hence, prism size.

* A real image exists at a specific location and can be shown on a screen. A virtual image can be observed by eye directly or reimaged by a lens, but it will not appear on a screen at that image's location.

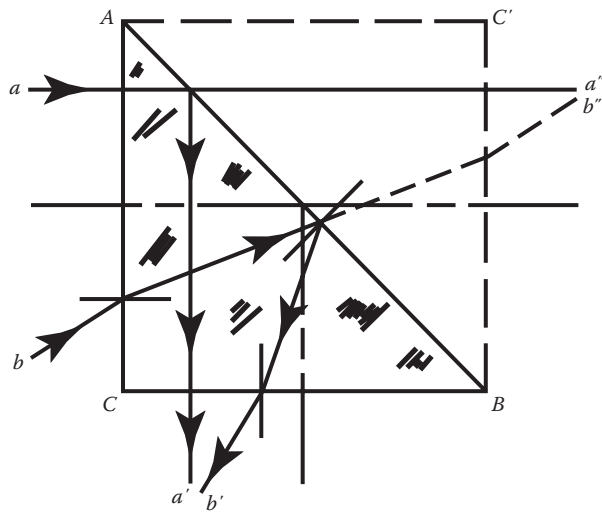


FIGURE 7.4
Tunnel diagram for a right-angle prism.

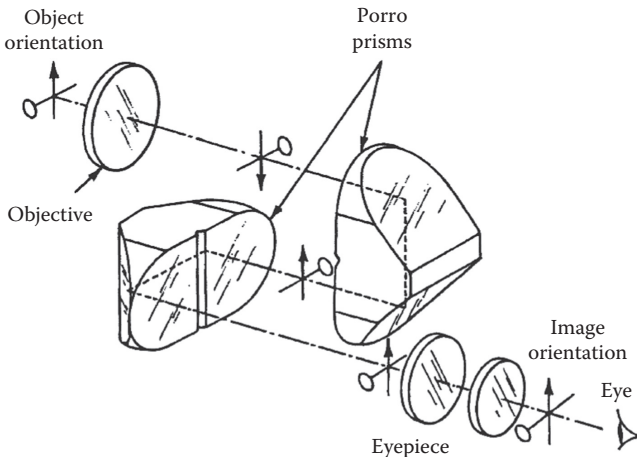
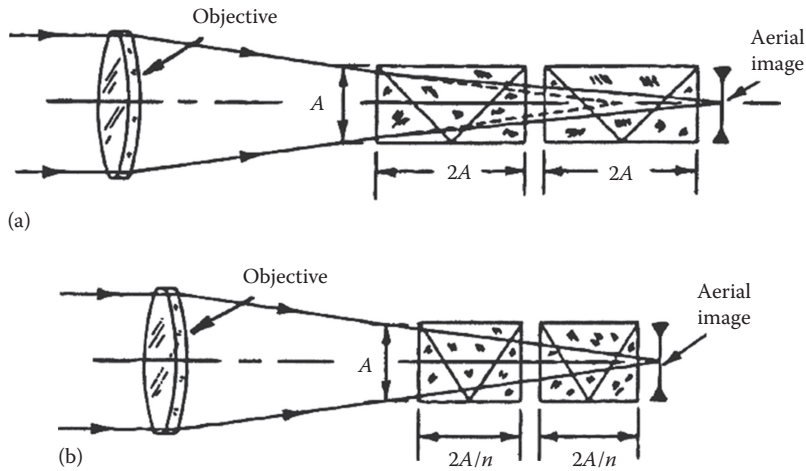


FIGURE 7.5
Optical system of a typical telescope with a Porro prism erecting system.

Figure 7.4 shows the tunnel diagram for a right-angle prism ABC . Rays $a-a''$ and $a-a'$ as well as $b-b''$ and $b-b'$ are symmetrical about the reflecting surface. To illustrate one use of a tunnel diagram, let us consider the telescope optical system shown in Figure 7.5. This might be a spotting telescope or one side of a binocular—each with a Porro prism erecting system. The prisms erect the image as indicated by the *arrow crossed with a drumstick* symbols at various locations in the figure. Figure 7.6 shows the front portion of this optical system with the prisms represented by tunnel diagrams. The diagonal lines indicate folds in the light path. In view (a), the conventional refracted path through each Porro prism is indicated by unfolding the path at each reflecting surface. For prisms of square face widths A (measured to sharp corners), the axial length of each prism is $2A$. In view (b), the tunnel diagrams are represented with axial lengths $2A/n$; these are the thicknesses of air optically equivalent to the paths through the glass plates. In the latter view, the marginal

**FIGURE 7.6**

Objective from Figure 7.5 with two Porro prisms shown by (a) conventional tunnel diagrams with refraction occurring at the air–glass interfaces and (b) tunnel diagrams with plane-parallel plates of air equivalent in thickness to the prisms that allow the rays to pass straight through. (Adapted from Smith, W.J., *Modern Optical Engineering*, 4th edn., McGraw-Hill, New York, 2008.)

rays converging to the axial image point are not refracted at the surfaces; they are drawn straight (undeviated) through the glass. To paraxial approximation, their intercepts on the prism surfaces are identical to the actual values.

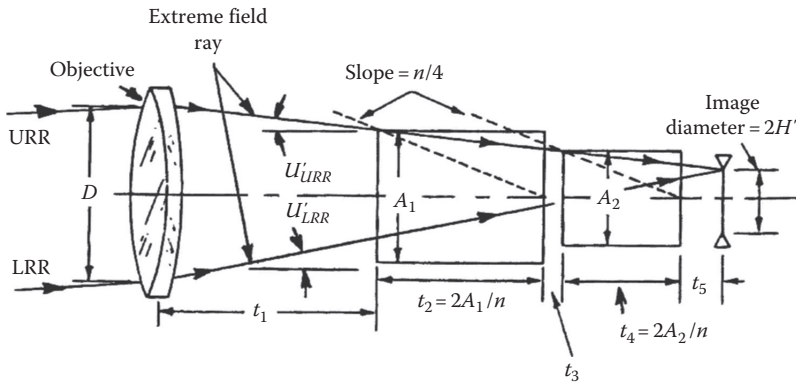
Smith (2008) used such a diagram to illustrate the computation of the minimum size Porro system that can be used in a 7×50 binocular without vignetting the extreme off-axis beam. He chose an objective focal length of 7 in. (177.8 mm) and an image diameter of 0.625 in. (15.88 mm). He noted from a figure similar to Figure 7.6b that the proportion of face width A_i to *equivalent air thickness* was $A_i : 2A_i/n_i$ or $n_{i/2}$. For $n = 1.5$, this ratio reduces to $1:2/1.5 = 3:4$. Smith then drew a diagram of the type shown in Figure 7.7 to illustrate the use of this ratio to define the minimum prism apertures A_1 and A_2 . The dashed lines drawn from the top front corners of the prisms to the opposite surface centers have slopes m of half the ratio just derived or $n_i/4$. These lines are the loci of the sharp corners of a family of prisms that have the proper proportions. The heights of the intersections of the dashed lines and the uppermost full-field ray (called the upper rim ray [URR] directed to the top of the image) locate the corners of the prisms. Note that the prism tunnel diagrams must be spaced along the optical axis with the design air spaces.

We see from Figure 7.7 that the slope of the URR is

$$\tan U'_{URR} = \frac{(D/2) - H'}{\text{EFL}_{OBJ}} \quad (7.6)$$

and the semiaperture of the second prism is $A_2/2 = H' + (t_4 + t_5)(\tan U')$. This semiaperture is also $A_2/2 = (m)(t_4) = (n_i)(t_4)/4$. Equating these expressions, we obtain the thickness t_4 of the second prism as

$$t_4 = \frac{(t_5 \tan U'_{URR}) + H'}{(n_i/4) - \tan U'_{URR}} \quad (7.7)$$

**FIGURE 7.7**

More detailed version of Figure 7.6b allowing the determination of minimum prism apertures from the geometric proportions of the prisms and extreme unvignetted rays for prism glass with $n = 1.5$. (Adapted from Smith, W.J., *Modern Optical Engineering*, 4th edn., McGraw-Hill, New York, 2008.)

Then, the second prism aperture is

$$A_2 = \frac{n_i t_4}{2} \quad (7.8)$$

Using similar logic, the expressions for the thickness and aperture of the first Porro prism are

$$t_2 = \frac{(t_3 + t_4 + t_5)(\tan U'_{URR}) + H'}{(n_i/4) - \tan U'_{URR}} \quad (7.9)$$

and

$$A_1 = \frac{n_i t_2}{2} \quad (7.10)$$

These approximations for the prism dimensions should be confirmed by geometric ray tracing. This is especially true if a specific amount of vignetting is needed for off-axis aberration control. The dimensions might well then be increased by a few percent to allow for protective bevels and dimensional tolerances before the design is considered final. The next design example shows the prism aperture calculation for a typical design.

Generally, in visual optical systems, optical surfaces such as the exit face of the second prism or the first surface of the eyepiece are kept at least 15 diopters away from the infinity image plane so that dust and surface imperfections, such as scratches or digs, are out of focus. In Smith's example, the eyepiece had a focal length of (objective EFL divided by the magnification) = $177.800/7.000 = 25.4$ mm (1.000 in.). One diopter of focus error would then be $(\text{eyepiece EFL})^2/39.37 = 0.645$ mm (0.025 in.). Fifteen diopters would then be 9.625 mm (0.375 in.). He chose an air space of 0.500 in. (12.700 mm), so the prism surface would be suitably out of focus to the observer's eye.

This same general geometric technique for aperture determination can be applied to other types of prisms used in converging or diverging light beams. The derivations of the

appropriate analytic equations for computing apertures in such applications are left to the reader. Once the prism apertures have been defined, we can determine the beam prints of the refracted beam on the prism's reflecting surfaces by an adaptation of the technique discussed in Section 9.2.4 for finding beam prints on mirrors. The primary difference is the use of the refracted ray slope inside the glass. Geometric ray tracing and many computer-aided design (CAD) programs can also define these beam prints.

7.2.4 Total Internal Reflection

When a light ray is incident at an interface where $n > n'$ (as, e.g., at the hypotenuse surface [surface 2] inside a right-angle prism), total internal reflection (TIR) can occur. In our discussion of tunnel diagrams, we assumed that all rays would reflect—as they would if the surface had a reflective coating such as silver or aluminum. Many people call such a surface a *silvered* surface. If the prism's hypotenuse surface is bare, however, Snell's law says that for small angles of incidence and/or low values of prism index, a ray can refract, that is, leak through that surface into the surrounding air (see ray $a-a'$ in Figure 7.8). This ray does not contribute to the image formed below the prism. If the ray angle I_2 increases, the angle I'_2 also increases. For some value of I_2 , I'_2 will reach 90° . Then $\sin I'_2$ is unity. Since this function cannot exceed unity, we find that rays with $I_2 > I_C$ will reflect internally, as if the surface were silvered. The value of I_2 corresponding to $I'_2 = 90^\circ$ is called the *critical angle*. It is abbreviated as I_C . This angle is calculated from

$$\sin I_C = \frac{n'}{n_2} \quad (7.11)$$

In air, $n' \approx 1.00029$, while in a vacuum, it is unity so $\sin I_C = 1/n_2$ to a very close approximation.

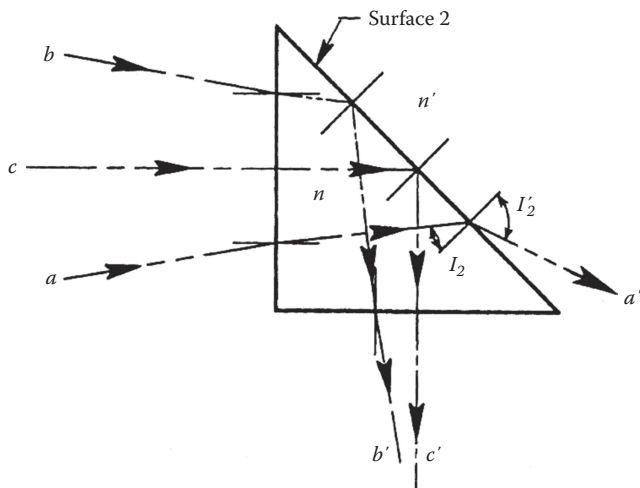


FIGURE 7.8

Ray paths through an unsilvered right-angle prism of low refractive index. Ray $a-a'$ is at an angle of incidence I_2 smaller than the critical angle I_C so it *leaks* through the surface, while I_2 for each of rays $b-b'$ and $c-c'$ exceeds I_C so they totally reflect internally.

DESIGN EXAMPLE 7.2 CALCULATION OF PORRO PRISM SIZE FOR A TELESCOPE ERECTING SYSTEM

Find the minimum apertures A_1 and A_2 for the prisms in an optical system as shown in Figure 7.7 if the EFL_{OBJ} is 177.800 mm (7.000 in), the objective aperture is 50.000 mm (1.968 in.), the image diameter is 15.875 mm (0.625 in.), the refractive index n of each prism is 1.620, t_3 is 3.175 mm (0.125 in.), and t_5 is 12.700 mm (0.500 in.).

From Equation 7.6,

$$\tan U'_{TIR} = [(50.000/2) \times (15.875/2)]/177.800 = 0.096, \quad \text{so } U'_{TIR} = 5.484^\circ$$

From Equation 7.7,

$$t_4 = [(12.700)(0.096) + (15.875/2)]/[(1.620/4) - 0.096] = 29.634 \text{ mm (1.167 in.)}$$

From Equation 7.8,

$$A_2 = (1.620)(29.634)/2 = 24.004 \text{ mm (0.945 mm)}$$

From Equation 7.9,

$$\begin{aligned} t_2 &= [(3.175 + 29.634 + 12.700)(0.096) + (15.875/2)]/[(1.620/4) - 0.096] \\ &= 12.307/0.309 = 39.828 \text{ mm (1.568 in.)} \end{aligned}$$

From Equation 7.10,

$$A_1 = (1.620)(39.828)/2 = 32.261 \text{ mm (1.270 in.)}$$

We can take advantage of TIR in prisms by choosing a refractive index high enough that the incidence angles for all rays that should reflect exceed I_C at the reflecting surface. Then, the reflections take place without photometric loss and reflective coatings are not needed on that surface. Because TIR occurs only on clean surfaces, special care must be taken not to let the reflecting surface become contaminated with condensed moisture, fingerprints, or foreign matter that can change the refractive index outside that surface and allow some useful rays to escape from the prism.

In the aforementioned discussion related to Figures 7.6, 7.7, and Design Example 7.2, we demonstrated how to determine the required apertures of Porro prisms used in an optical system such as that shown in Figure 7.5. Another calculation that should be done during the preliminary design of a telescope if unsilvered Porro prisms are to be used is illustrated in Design Example 7.3. There, we determine the largest field of view that can be provided by the system without vignetting any rays due to inadequate refractive index of the prisms.

A consequence of using prisms made of glass with refractive index too small for all desired rays to reflect by TIR is evident in some telescopes and binoculars. This is especially true in many older designs and low-cost contemporary units. Such instruments can be identified rather easily by holding the instrument ~30 cm (~12 in.) in front

DESIGN EXAMPLE 7.3 MAXIMUM FIELD OF VIEW FOR A TELESCOPE USING UNSILVERED PORRO PRISMS

Assume that the prisms shown in Figures 7.5 and 7.6 are not silvered, are in air, and have refractive indices of 1.620. The objective focal length is 177.800 mm (7.000 in.) and its entrance pupil diameter D is 50.000 mm (1.969 in.). What is the maximum circular field of view in object space that can be seen through the telescope without vignetting due to loss of TIR? Assume the aperture stop to be at the objective.

From Equation 7.11,

$$\sin I_C = 1/1.620 = 0.617 \text{ and } I_C = 38.118^\circ$$

From the geometry of Figure 7.4,

$$I' \text{ for ray } a-a' \text{ at the entrance face is } (45^\circ - I_C) = 6.882^\circ$$

From Equation 7.1,

$$\sin I = (1.620)(\sin 6.882^\circ) = 0.194, \text{ so } I = 11.193^\circ$$

This angle equals the slope of the LRR entering the bottom of the lens aperture and aimed toward the top of the image. Hence, $U'_{PR} = 11.193^\circ$ and $\tan U'_{PR} = 0.198$.

Modifying Equation 7.6 to apply to the LRR (by changing the minus sign to a plus sign in the numerator), we get

$$\tan U'_{PR} = [(50.000/2) + H']/177.800 = 0.198$$

Solving for the image height, $H' = 10.183$ mm (0.401 in.)

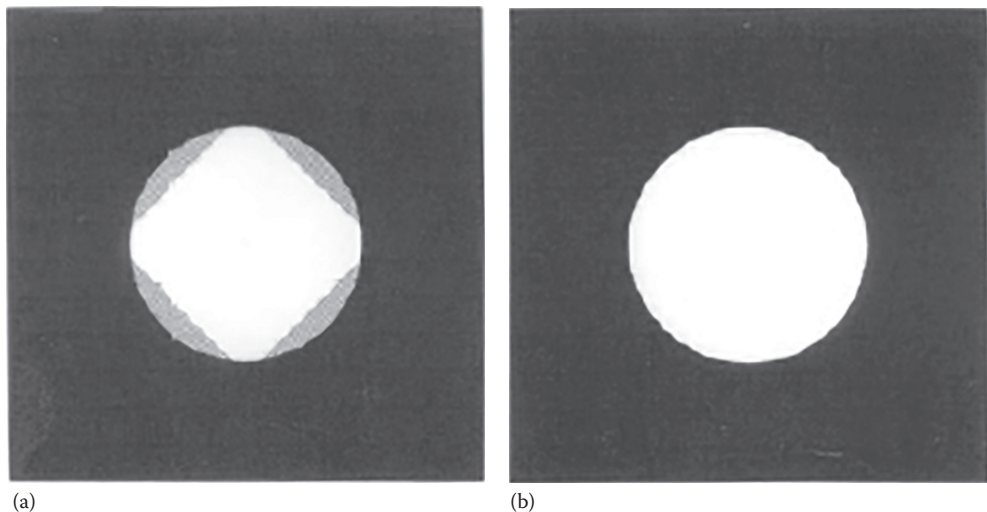
$$\text{Paraxially, } H' = (\text{EFL}_{OBJ})(\tan U'_{PR}) \quad (7.12)$$

Hence, the total unvignetted telescope circular field of view in object space (sometimes called the real field) is

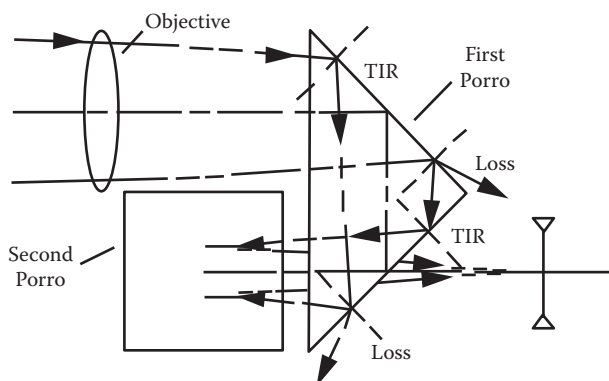
$$\pm\tan^{-1}(H'/\text{EFL}_{OBJ}) = \pm3.278^\circ \text{ or a total of } 6.556^\circ$$

of the eye, pointing it toward a bright surface or the daytime sky (but not at the sun!) and looking at its exit pupil approximately along the eyepiece axis. If the glass index is too low, the edge of the exit pupil will be *squared off* somewhat as shown at the left in Figure 7.9 rather than completely circular as seen at the right in the figure. This indicates that some light is leaking through each glass-air interface in the first prism as shown in Figure 7.10. The same thing happens at two reflecting surfaces in the second Porro prism so four parts of the transmitted light beam located at 90° intervals about the axis are vignetted.

Referring once again to Figure 7.10, we see that the rays entering the objective are parallel to each other and to the axis. Hence, they originate at a distant point on axis. They are often referred to as marginal rays because they enter at the margins of the lens aperture.

**FIGURE 7.9**

Views of exit pupils from a telescope or binocular with Porro prisms made of (a) low refractive index causing vignetting to *square* pupil shape and (b) higher-index prisms resulting in an unvignetted round pupil. (From Yoder, P.R., Jr. and Vukobratovich, D., *Field Guide for Binoculars and Scopes*, SPIE Press, Bellingham, WA, 2011.)

**FIGURE 7.10**

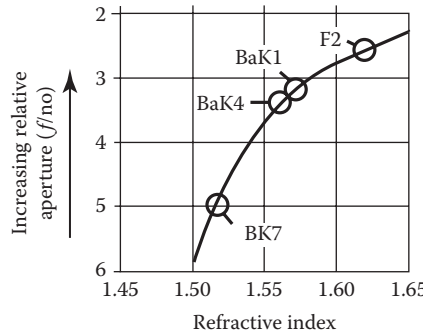
Ray paths through Porro prisms with inadequate refractive index causing partial loss of TIR at four reflecting surfaces and causing vignetted *square* exit pupils. (From Yoder, P.R., Jr. and Vukobratovich, D., *Field Guide for Binoculars and Scopes*, SPIE Press, Bellingham, WA, 2011.)

After the lens, they converge to an axial point image. Their total angle of convergence is proportional to the relative aperture, *speed*, or *f-number* of the beam. The latter is expressed as*

$$f\text{-Number} = \frac{\text{EFL}}{\text{Lens entrance pupil (EP) aperture}} \quad (7.13)$$

For example, a 177.800 mm (7.000 in.) EFL lens with an EP of 40.000 mm (1.575 in.) is *f/4.4*. If the beam is not vignetted, the square of this ratio determines the illuminance of the

* The entrance pupil is the image of the aperture stop as seen from object space. The aperture stop is the mechanical aperture that limits the size of the light beam passing through an optical system.

**FIGURE 7.11**

Plot of objective lens limiting relative aperture in a telescope or binocular optical system with Porro prisms made of glasses having different refractive indices. Circles represent specific frequently used glasses. Higher-index glass allows faster, that is, more compact, objective designs free of vignetting that causes square exit pupils. (From Yoder, P.R., Jr. and Vukobratovich, D., *Field Guide for Binoculars and Scopes*, SPIE Press, Bellingham, WA, 2011.)

image for a given object luminance. Atmospheric effects are here ignored. With vignetting, the image luminance is reduced by the ratio of the unvignetted area to the total aperture area.

During the design of a telescope with Porro prisms that could vignette the beam as described earlier, if the refractive index is too low, it is desirable to know what *f*-number the system can have without causing this vignetting. The curve in Figure 7.11 shows this relationship. The indices for four high-quality glass types typical of those used in binoculars and telescopes are indicated. BK7 represents a borosilicate crown with index *n* of 1.517 that was used in older designs and lower-cost instruments today. With that glass, the lens must be *f*/5 or slower to ensure TIR for the entire beam. The chosen glass for many newer designs is BaK4 with *n* = 1.569. It allows the lenses to be *f*/3.2 and produce a shorter optical system. The other glasses, BaK1, with *n* = 1.573 and F2 with *n* = 1.620, represent glasses of choice for other designs. They allow beam *f*-numbers of ~3.2 and ~2.6, respectively.

7.2.5 Aberrations Caused by Prisms and Plates

Many plates and internally reflecting prisms are designed so that entrance and exit faces are both perpendicular to the optical axis of the transmitted beam. If the beam is collimated and passes through the optic normal to the entrance and exit faces, no aberrations are introduced. Aberrations are introduced if the beam is divergent or convergent; they become asymmetric if the beam enters the prism at an angle to the axis. In a converging beam, a prism overcorrects the three longitudinal aberrations (spherical, chromatic aberration, and astigmatism) while it undercorrects the transverse aberrations (coma, distortion, and lateral color). Smith (2008) provided both exact and paraxial equations for computing the aberration contributions of a generic prism, with index of refraction *n* by defining it as a thick plane-parallel plate of thickness *t* oriented with the surfaces normal to the axis or tilted through some angle relative to the axis. These aberrations can also be determined by surface-by-surface ray tracing in a lens design code. The interested reader is referred to Smith's explanation of both these subjects.

7.3 Beam-Folding Prisms

7.3.1 Right-Angle Prism

The right-angle prism folds a light beam by 90° , as shown in the tunnel diagram of Figure 7.4. Figure 7.12a shows three views of this type of prism. Figure 7.12b shows the path of a ray entering at maximum I_1 for TIR at Surface 2. This prism and all others considered in this chapter are assumed to be in air with $n_1 = 1.000$. Dimensions are measured to sharp corners. Design Example 7.4 provides equations for the dimensions and angles indicated in the figure as well as computed values for the indicated set of prism parameters.

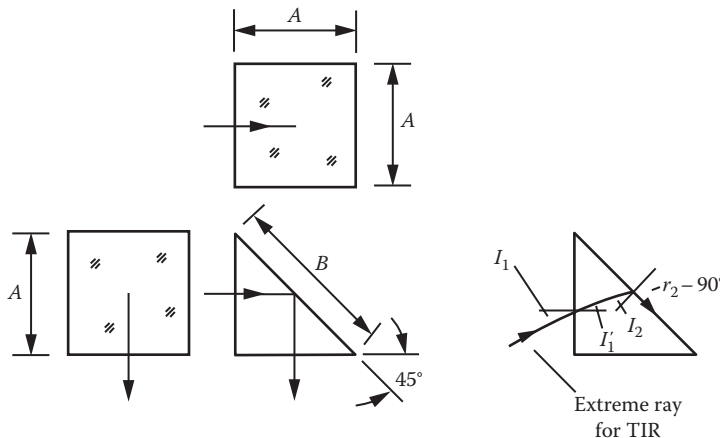


FIGURE 7.12

Configuration of a typical right-angle prism.

**DESIGN EXAMPLE 7.4 RIGHT-ANGLE PRISM OF APERTURE
 $A = 38.100 \text{ mm}$, $n_2 = 1.517$, AND $\rho = 2.510 \text{ g/cm}^3$ (SEE FIGURE 7.12)**

Parameter	Equation Number
$t_A = A = 38.100 \text{ mm}$ (1.500 in.)	(7.14)
$B = 1.414A = 53.873 \text{ mm}$ (2.121 in.)	(7.15)
$I_C = \sin^{-1}(1/n_2) = 41.239^\circ$	(7.16)
$I'_1 = 45^\circ - I_C = 3.761^\circ$	(7.17)
$I_1 = \sin^{-1}[(n_2/n_1)(\sin I'_1)] = 5.711^\circ$	(7.1)
$V = (0.5) A^3/1000 = 27.653 \text{ cm}^3$ (1.688 in. ³)	(7.18)
$W = V\rho/1000 = 0.069 \text{ kg}$ (0.153 lb)	(7.19)

7.3.2 Beam Splitter (or Beam Combiner) Cube Prism

Two right-angle prisms with their hypotenuse surfaces cemented together and a partially reflective coating in that interface form a cube-shaped beam splitter or beam combiner. This type of prism is shown in Figure 7.13. Design equations and typical computations are given in the following Design Example 7.5.

As is usually the case for optical reasons, it is assumed in this chapter that prisms to be joined together are made of the same material in order to avoid adverse effects from temperature changes.

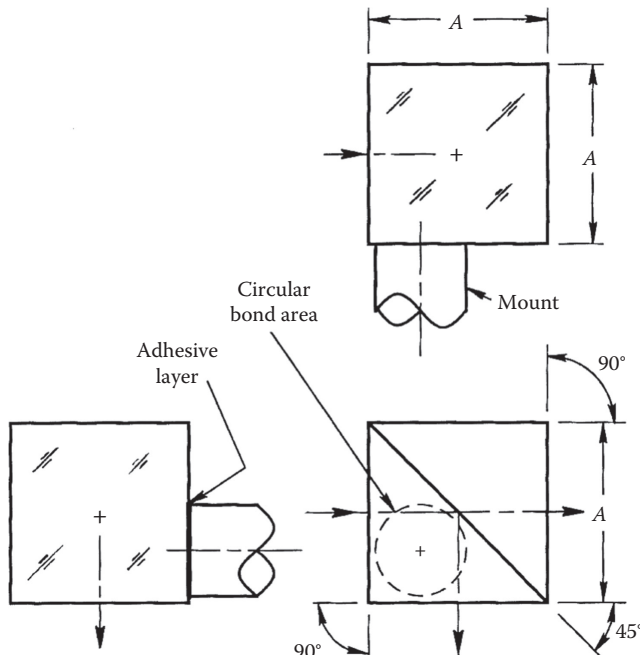


FIGURE 7.13
Configuration of a typical beam splitter or beam combiner cube prism.

**DESIGN EXAMPLE 7.5 BEAM SPLITTER (OR BEAM COMBINER)
CUBE PRISM OF APERTURE $A = 38.100 \text{ mm}$, $\rho = 2.510 \text{ g/cm}^3$,
 $A_G = 10$, $F_s = 10$, AND $J = 13.790 \text{ MPa}$ (SEE FIGURE 7.13)**

Parameter	Equation Number
$t_A = A = 38.100 \text{ mm} (1.500 \text{ in.})$	(7.14)
$V = A^3/1000 = 55.306 \text{ cm}^3 (3.375 \text{ in.}^3)$	(7.20)
$W = V\rho/1000 = 0.139 \text{ kg} (0.305 \text{ lb})$	(7.19)

If the beam splitter/combiner prism (or any multiple-component prism) is to be bonded to a mechanical mounting, the adhesive joint should be applied to only one component. The bond would then not bridge the cemented joint. This is because the two glass surfaces may not be accurately coplanar and the strength of the bond may be degraded by differences in adhesive thickness. If the adjacent surfaces are reground coplanar after cementing, bonding across the joint *may* be acceptable.

The design equations for the beam splitter cube also apply to a monolithic cube that might be used as a rotating prism in some types of high-speed cameras.

7.3.3 Rhomboid Prism

The rhomboid prism shown in Figure 7.14 is equivalent to a combination of two right-angle prisms of aperture A with their reflecting surfaces of face length D parallel. Integral with and between these prisms may be a plane-parallel plate of dimensions $A \times A \times C$. The prism is used to displace the axis transversely by a distance B without changing the axis direction. An image seen through such a device is erect in both directions. The following Design Example 7.6 and equations given therein pertain.

The rhomboid prism is subject to the same light leakage problem as described for the right-angle prism (see the right-hand view of Figure 7.12) if the index is not high enough to ensure that TIR and the reflecting surfaces are not given reflecting coatings such as aluminum or silver.

This prism is insensitive to tilt about any axis normal to the plane of reflection, so it provides constant deviation in that plane. Rotations about the long axis of the prism result in

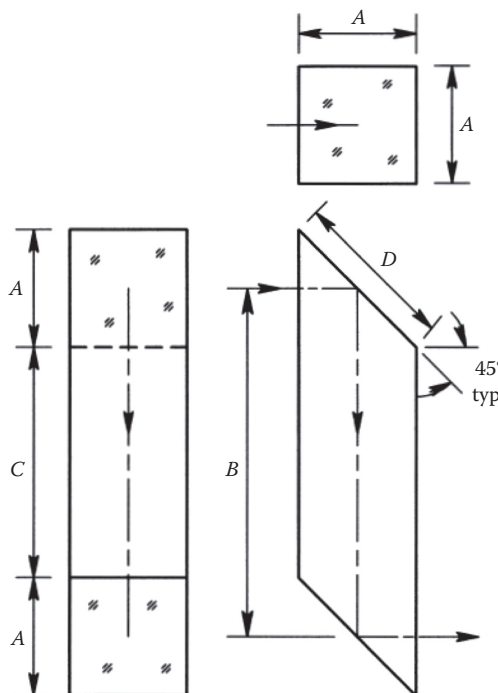


FIGURE 7.14
Configuration of a typical rhomboid prism.

**DESIGN EXAMPLE 7.6 RHOMBOID PRISM OF APERTURE
 $A = 38.100 \text{ mm}$ AND $\rho = 2.510 \text{ g/cm}^3$ (SEE FIGURE 7.14)**

Parameter	Equation Number
$B \equiv 135.000 \text{ mm}$ (5.315 in.)	Chosen value
$t_A = A + B = 173.100 \text{ mm}$ (6.815 in.)	(7.21)
$C = B - A = 135.000 - 38.100 = 96.900 \text{ mm}$ (3.815 in.)	(7.22)
$D = 1.414A = (1.414)(38.100) = 53.873 \text{ mm}$ (2.121 in.)	(7.23)
$E = 2A + C = (2)(38.100) + 96.900 = 173.100 \text{ mm}$ (6.815 in.)	(7.24)
$V = (A^3 + A^2 C)/1000$ $= [55,306.341 + (1451.610)(96.900)]/1000 = 195.967 \text{ cm}^3$ (11.959 in. ³)	(7.25)
$W = V\rho/1000 = (195.967)(2.510)/1000 = 0.492 \text{ kg}$ (1.082 lb)	(7.19)

the usual relationship of 2:1 beam deviation versus reflecting surface rotation. The rhomboid prism is frequently used in periscopes in military applications to translate the line of sight transversely in order that targets might be seen from entrenchments, from behind obstructions or from within enclosures such as armored vehicles.

7.3.4 Porro Prism

A right-angle prism oriented so that the beam enters and exits the hypotenuse surface, as shown in Figures 7.5 and 7.15, is called a *Porro prism*. In the left-hand view of the latter figure, ray $a-a'$ enters and exits parallel to the axis, while rays $b-b'$ and $c-c'$ enter the prism at different field angles. Note that rays $a-a'$ and $b-b'$ turn around 180° and exit through the hypotenuse. If the 90° angle is exact, these exiting rays are parallel to the corresponding entering rays. This is true even if the prism is rotated about any axis normal to face $A-B-C$. Hence, the prism is retrodirective and provides constant deviation in the plane of reflection. Prism rotation about an axis parallel to edge $A-C$ results in deviation of the reflected beam out of the plane of the figure by twice the prism rotation angle, just like a mirror would behave.

Ray $c-c'$ in Figure 7.15 represents a field ray entering near the edge of the prism aperture. After the first reflection, it intercepts the hypotenuse surface $A-C$ at grazing incidence. Because it ultimately has three reflections, it produces an inverted image. Such a ray is called a *ghost ray* because it does not contribute useful information to the main image. It also adds stray light. This ray and many following similar paths can be blocked by the groove cut across the center of the hypotenuse surface. This groove does not interfere with the useful rays passing through the prism.

This prism (see Figure 7.16) is geometrically equivalent to two right-angle prisms of aperture $A \times A$ with square refracting faces connected by a plane-parallel plate of dimensions $A \times A \times D$ centered between the right-angled elements. Design equations and typical dimensions are provided in Design Example 7.7.

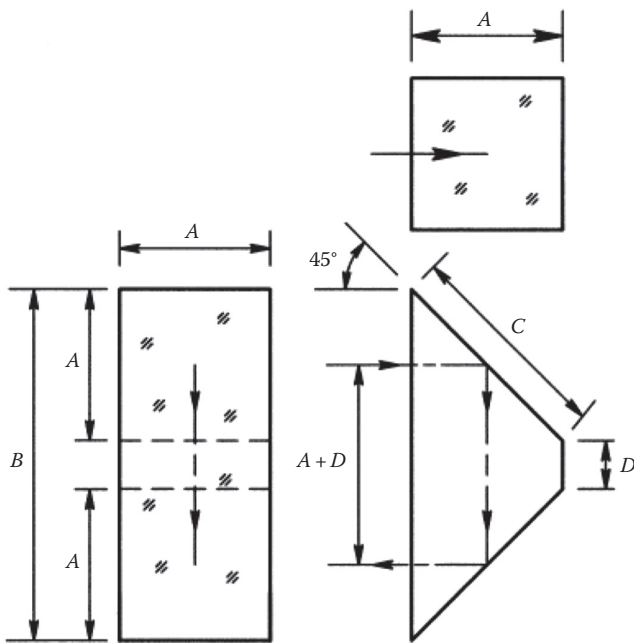


FIGURE 7.15
Configuration of a typical Porro prism.

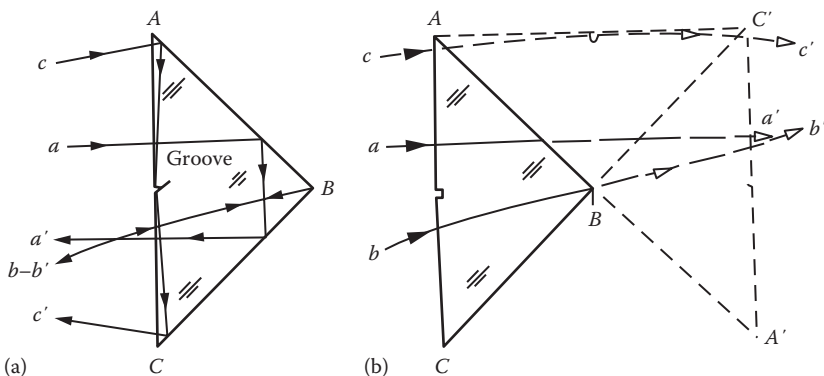


FIGURE 7.16
(a) Typical ray paths through a Porro prism. (b) The prism's tunnel diagram.

7.3.5 Abbe–Porro Prism

Ernst Abbe modified the configuration of the Porro prism by designing it so one-half of the prism is rotated by 90° with respect to the other half. This prism is sometimes referred to as a *Type 2 Porro prism*. Figure 7.17 illustrates the prism. Design equations and typical dimensions are provided in Design Example 7.8. Note that the results for these examples are identical because the difference in configuration between the prisms does not change the dimensions nor the applicable equations.

**DESIGN EXAMPLE 7.7 PORRO PRISM WITH APERTURE
 $A = 38.100 \text{ mm}$, AND $\rho = 2.510 \text{ g/cm}^3$ (SEE FIGURE 7.15)**

Parameter	Equation Number
$D = 0.24A = 9.144 \text{ mm}$ (0.360 in.)	Chosen value
$t_A = 2A + D = 85.344 \text{ mm}$ (3.360 in.)	(7.26)
$B = 2A + D = 85.344 \text{ mm}$ (3.360 in.)	(7.27)
$C = 1.414A = 53.873 \text{ mm}$ (2.121 in.)	(7.28)
$V = (A^3/1000) + (A^2D/1000) = 68.580 \text{ cm}^3$ (4.185 in. ³)	(7.29)
$W = V\rho/1000 = (68.580)(2.510)/1000 = 0.172 \text{ kg}$ (0.379 lb)	(7.19)

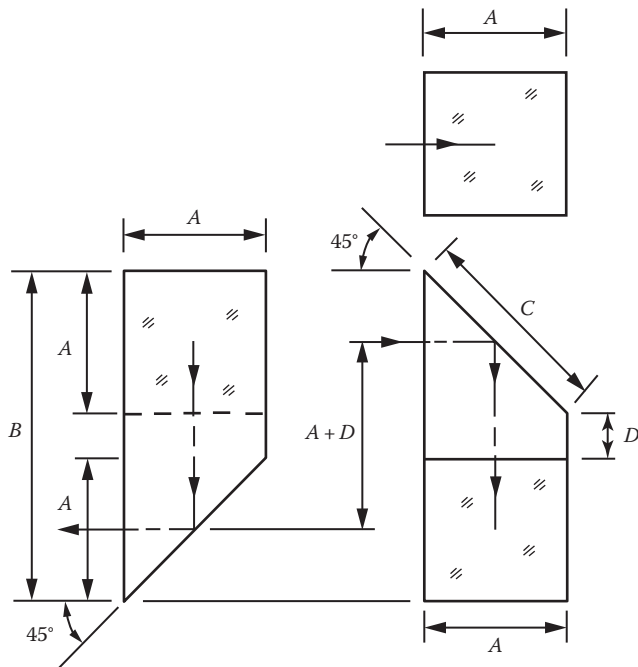


FIGURE 7.17
 Configuration of the Abbe version of a Porro prism.

7.3.6 Amici Prism

The Amici prism (see Figure 7.18) is a right-angle prism of aperture A with its hypotenuse shaped into a 90° roof. The reflected beam then undergoes two reflections instead of just one. The transmitted image is inverted in the direction normal to the plane of the lower right view in the figure (see Design Example 7.9).

**DESIGN EXAMPLE 7.8 ABBE-PORRO PRISM WITH APERTURE
 $A = 38.100 \text{ mm}$ AND $\rho = 2.510 \text{ g/cm}^3$ (SEE FIGURE 7.17)**

Parameter	Equation Number
$D = 0.05A = 1.905 \text{ mm}$ (0.075 in.)	Chosen value
$t_A = 2A + D = 78.105 \text{ mm}$ (3.075 in.)	(7.26)
$B = 2A + D = 78.105 \text{ mm}$ (3.075 in.)	(7.27)
$C = 1.414A = 53.873 \text{ mm}$ (2.121 in.)	(7.28)
$V = (A^3/1000) + (A^2D/1000) = 58.071 \text{ cm}^3$ (3.544 in. ³)	(7.29)
$W = V\rho/1000 = (58.07)(2.510)/1000 = 0.156 \text{ kg}$ (0.071 lb)	(7.19)

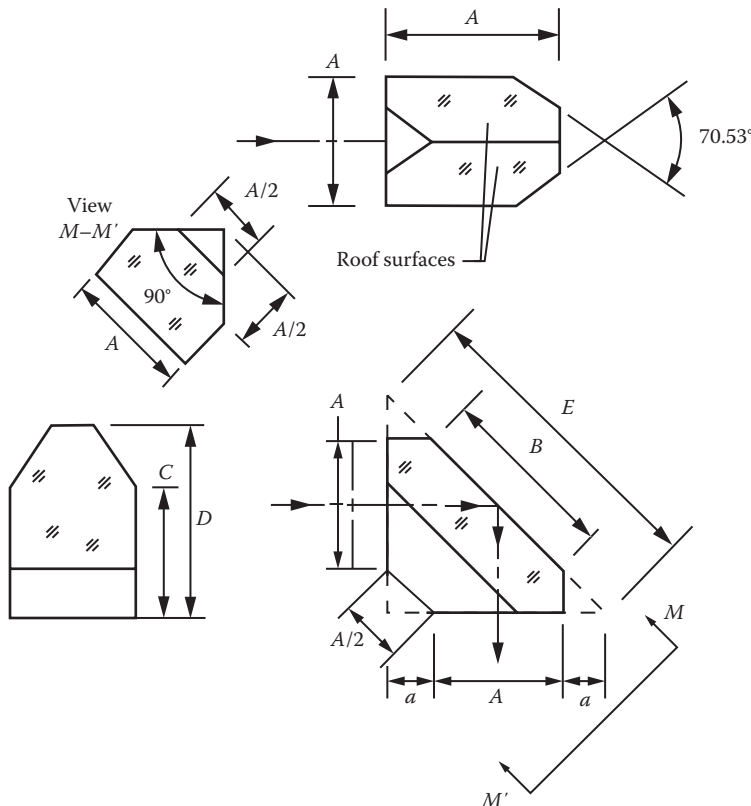


FIGURE 7.18
 Configuration of a typical Amici prism.

**DESIGN EXAMPLE 7.9 AMICI PRISM OF APERTURE
 $A = 38.100 \text{ mm}$ AND $\rho = 2.510 \text{ g/cm}^3$ (SEE FIGURE 7.18)**

Parameter	Equation Number
$t_A = 1.708A = 65.075 \text{ mm}$ (2.562 in.)	(7.30)
$a = 0.354A = 13.487 \text{ mm}$ (0.531 in.)	(7.31)
$B = 1.414A = 53.881 \text{ mm}$ (2.021 in.)	(7.15)
$C = 0.854A = 32.537 \text{ mm}$ (1.281 in.)	(7.32)
$D = 1.354A = 51.587 \text{ mm}$ (2.031 in.)	(7.33)
$E = 1.440A = 54.882 \text{ mm}$ (2.161 in.)	(7.34)
$V = 0.888A^3/1000 = 49.112 \text{ cm}^3$ (2.997 in. ³)	(7.35)
$W = V\rho/1000 = (49.112)(2.510)/1000 = 0.123 \text{ kg}$ (0.271 lb)	(7.19)

This prism can be used in such a manner that the transmitted beam is split by the dihedral edge between the roof surfaces or, with a larger prism but constant beam size, so the beam hits the roof surfaces separately and in sequence. These possibilities are illustrated in Figure 7.19a and b, respectively. If the beam is split, the dihedral angle must be accurately 90° (typically within a few arcseconds) in order not to produce a noticeable double image. This generally increases the cost of the prism because of the added labor and fixturing required to perfect the roof angle.*

The prisms of Figure 7.19 are drawn with the same entrance aperture sizes, so the beam in view (a) can be almost as large as the prism aperture A and is centered. The beam in view (b) cannot be larger than $A/2$. The beam axis is displaced laterally by $A/2$ in this case as the beam reflects from one roof face and then the other roof face.

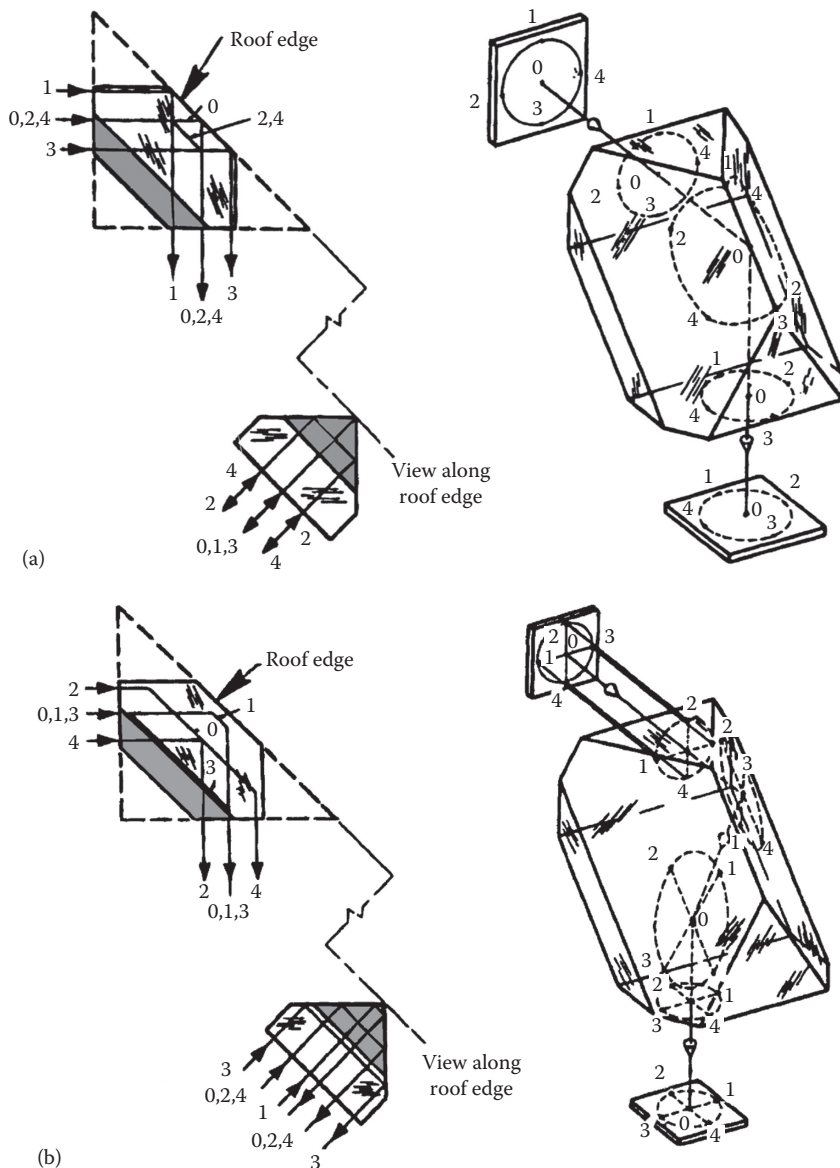
7.3.7 Frankford Arsenal Type 1 and Type 2 Prisms

These prisms resemble and function similarly to the Amici prism but deviate the incident beam by 115° and 60° , respectively, rather than 90° . Figure 7.20a and b shows their configurations. Design Examples 7.10 and 7.11 for these prisms follow.

7.3.8 Penta Prism

The penta prism neither reverts nor inverts the image; it merely turns the axis by exactly 90° . Its configuration is defined in Figure 7.21. It provides constant deviation in the plane of the figure. Common applications include optical range finders, surveying equipment, optical alignment systems, and metrology equipment where high accuracy of the 90° deviation is essential. The reflecting surfaces do not provide TIR, so they must have reflecting coatings. We show Design Example 7.12 with prism dimension calculations for a typical case.

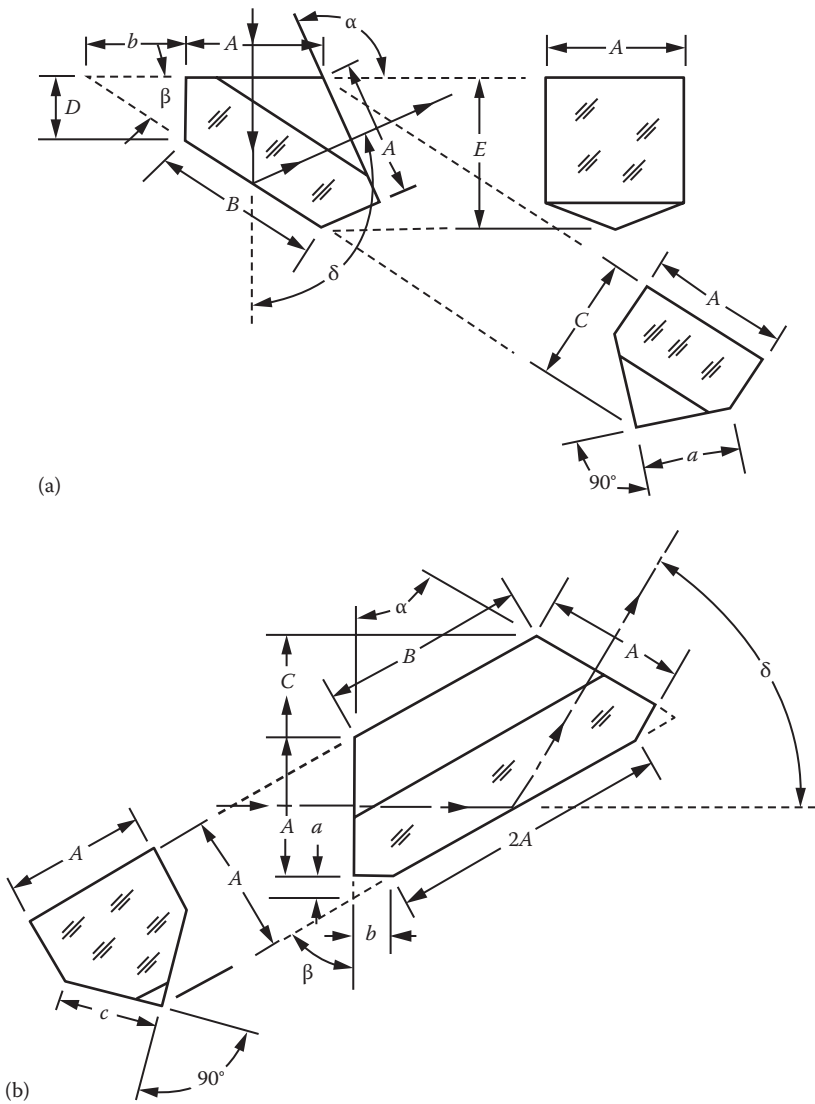
* The two reflections from the roof surfaces in any roof prism cause a polarization-dependent phase shift between the two beams resulting in a reduction in image quality from interference. This effect is compensated by coating one surface of the roof with a thin-film coating that brings the two reflections back into phase.

**FIGURE 7.19**

The Amici prism used (a) symmetrically as a split-beam reflector and (b) off-center as a full-beam reflector. (From MIL-HDBK-141, *Optical Design*, Defense Supply Agency, Washington, DC, 1962.)

7.3.9 Roof Penta Prism

If we configure one reflecting surface of a penta prism as a precise 90° roof, the prism inverts the transmitted image in the direction normal to the plane of refraction. For a given aperture and material, the roof penta's volume and weight are about 20% greater than the conventional penta. Adding the roof does not change the penta prism's constant-deviation characteristic. The roof penta is shown in Figure 7.22. Design Example 7.13 summarizes this design.

**FIGURE 7.20**

Configurations of (a) Frankford Arsenal Prism No. 1 and (b) Frankford Arsenal Prism No. 2. (Adapted from Kaspereit, O.K., *Design of Fire Control Optics ORDM 2-1*, Vol. I, U.S. Army, Washington, DC, 1953.)

7.3.10 45° Bauernfeind Prism

The Bauernfeind prism (see Figure 7.23) provides a 45° deviation of the axis using two internal reflections. The first reflection is by TIR for small fields of view, but the second requires a reflecting coating because the angle of incidence is too small for TIR. It is used as the smaller element in the Pechan prism (see Section 7.5.4) and is geometrically the same as one-half of a penta prism. It then may be called a *half penta prism*. Design Example 7.14 describes a specific design for this type of prism. A 60° deviation version of this prism has been used in some applications.

**DESIGN EXAMPLE 7.10 FRANKFORD ARSENAL TYPE 1
PRISM OF APERTURE $A = 38.100$ mm (SEE FIGURE 7.20a)**

Parameter	Equation Number
$\alpha = \delta = 115^\circ$	Given
$\beta = 32.5^\circ$	Given
$t_A = 1.570A = 59.817$ mm (2.355 in.)	(7.36)
$a = 0.707A = 26.937$ mm (1.061 in.)	(7.37)
$b = 0.732A = 27.889$ mm (1.098 in.)	(7.38)
$B = 1.186A = 45.187$ mm (1.770 in.)	(7.39)
$C = 0.931A = 35.471$ mm (1.397 in.)	(7.40)
$D = 0.461A = 17.564$ mm (0.692 in.)	(7.41)
$E = 1.104A = 42.062$ mm (1.656 in.)	(7.42)

Source: Kaspereit, O.K., *Design of Fire Control Optics ORDM 2-1*, Vol. I, U.S. Army, Washington, DC, 1953.

**DESIGN EXAMPLE 7.11 FRANKFORD ARSENAL TYPE 2
PRISM OF APERTURE $A = 38.100$ mm (SEE FIGURE 7.20b)**

Parameter	Equation Number
$\alpha = \beta = \delta = 60^\circ$	Given
$t_A = 2.269A = 86.449$ mm (3.404 in.)	(7.43)
$a = 0.155A = 5.906$ mm (0.233 in.)	(7.44)
$b = 0.268A = 10.211$ mm (0.402 in.)	(7.45)
$c = 0.707A = 26.949$ mm (1.061 in.)	(7.46)
$B = 1.464A = 55.778$ mm (2.196 in.)	(7.47)

Source: Kaspereit, O.K., *Design of Fire Control Optics ORDM 2-1*, Vol. I, U.S. Army, Washington, DC, 1953.

7.4 Image Erecting Prisms

In this section, we describe prism arrangements or systems that will reorient the inverted (up down) and reverted (left right) image formed by a lens so that it appears to an observer in the same orientation as the object. Each of these prisms has an even number of reflections in both meridians.

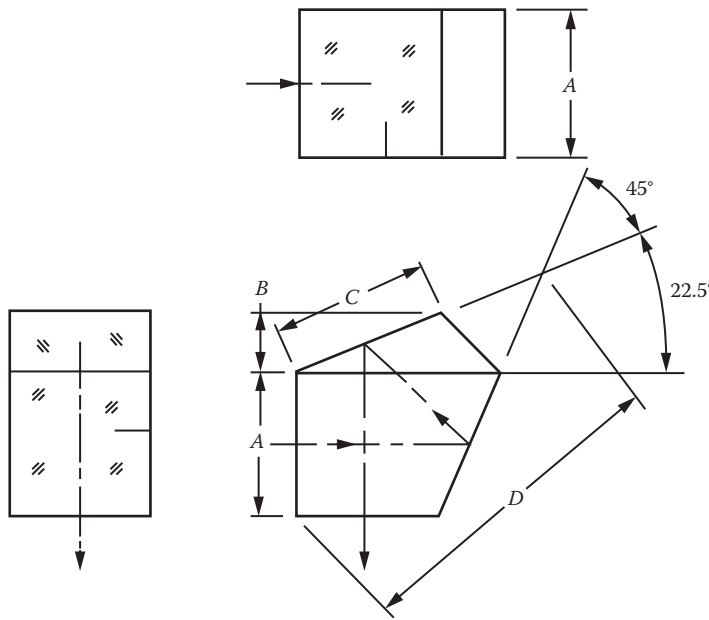


FIGURE 7.21
Configuration of a typical penta prism.

**DESIGN EXAMPLE 7.12 PENTA PRISM OF APERTURE
 $A = 38.100 \text{ mm}$ AND $\rho = 2.510 \text{ g/cm}^3$ (SEE FIGURE 7.21)**

Parameter	Equation Number
$t_A = 3.414A = 130.073 \text{ mm}$ (5.121 in.)	(7.48)
$B = 0.414A = 15.773 \text{ mm}$ (0.621 in.)	(7.49)
$C = 1.082A = 41.224 \text{ mm}$ (1.623 in.)	(7.50)
$D = 2.414A = 91.973 \text{ mm}$ (3.621 in.)	(7.51)
$V = 1.500A^3 = 82.951 \text{ cm}^3$ (5.062 in. ³)	(7.52)
$W = V\rho/1000 = (82.951)(2.510)/1000 = 0.208 \text{ kg}$ (0.095 lb)	(7.19)

7.4.1 Porro Erecting System

Two Porro prisms of equal apertures A oriented at 90° to each other and air spaced as shown in Figure 7.5 or cemented together, as shown in Figure 7.24, constitute a Porro erecting system. The axis is displaced laterally in each transverse direction by A plus the thickness D of the integral plane-parallel plate usually located between the right-angle prisms (see Figure 7.16). Design Example 7.15 pertains to a cemented assembly. This type of erector is most frequently used in binoculars and small telescopes. It is not a constant-deviation prism subassembly, so movements or misalignments of the subassembly will displace the transmitted beam.

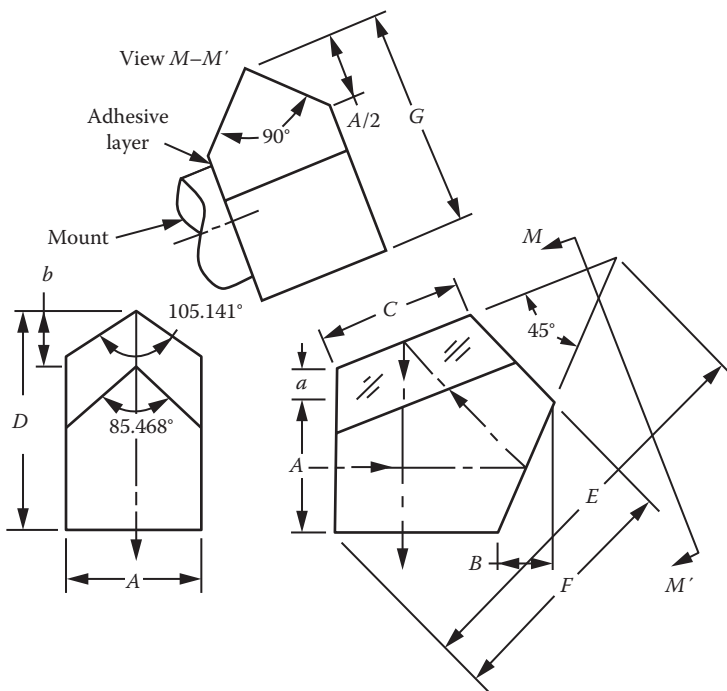


FIGURE 7.22
Configuration of a typical roof penta prism.

**DESIGN EXAMPLE 7.13 ROOF PENTA PRISM OF APERTURE
 $A = 38.100 \text{ mm}$ AND $\rho = 2.510 \text{ g/cm}^3$ (SEE FIGURE 7.22)**

Parameter	Equation Number
$t_A = 4.223A = 160.896 \text{ mm (6.334 in.)}$	(7.53)
$a = 0.237A = 9.030 \text{ mm (0.355 in.)}$	(7.54)
$b = 0.414A = 15.773 \text{ mm (0.621 in.)}$	(7.55)
$B = 0.414A = 15.773 \text{ mm (0.621 in.)}$	(7.49)
$C = 1.082A = 41.224 \text{ mm (1.623 in.)}$	(7.50)
$D = 1.651A = 62.903 \text{ mm (2.476 in.)}$	(7.56)
$E = 2.986A = 113.767 \text{ mm (4.479 in.)}$	(7.57)
$F = 1.874A = 71.399 \text{ mm (2.811 in.)}$	(7.58)
$G = 1.621A = 61.760 \text{ mm (2.431 in.)}$	(7.59)
$V = 1.795A^3/1000 = 99.275 \text{ cm}^3 (6.058 \text{ in.}^3)$	(7.60)
$W = V\rho/1000 = (99.275)(2.510)/1000 = 0.250 \text{ kg (0.552 lb)}$	(7.19)

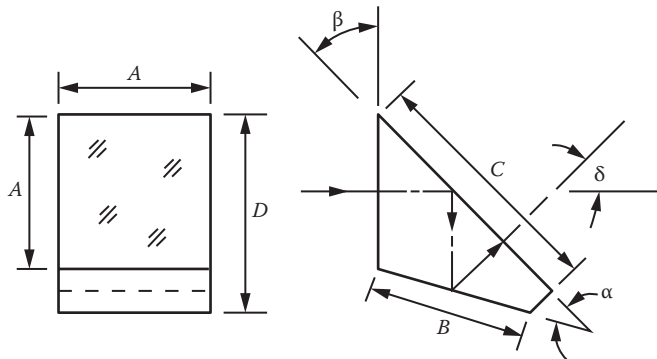


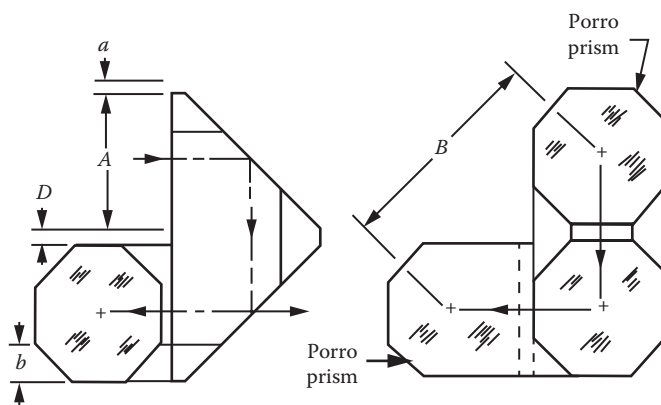
FIGURE 7.23
Configuration of a 45° Bauernfeind prism.

**DESIGN EXAMPLE 7.14 45° BAUERNFEIND PRISM OF APERTURE
 $A = 38.100 \text{ mm}$ AND $\rho = 2.510 \text{ g/cm}^3$ (SEE FIGURE 7.23)**

Parameter	Equation Number
$\alpha = 22.5^\circ$	Given
$\beta = 45^\circ$	Given
$\delta = 45^\circ$	Given
$t_A = 1.707A = 65.040 \text{ mm} (2.561 \text{ in.})$	(7.61)
$B = 1.082A = 41.224 \text{ mm} (1.623 \text{ in.})$	(7.62)
$C = 1.707A = 65.040 \text{ mm} (2.561 \text{ in.})$	(7.63)
$D = 2.414A = 91.981 \text{ mm} (3.621 \text{ in.})$	(7.51)
$V = 0.750A^3/1000 = 41.480 \text{ cm}^3 (2.121 \text{ in.}^3)$	(7.64)
$W = V\rho/1000 = (41.480)(2.510)/1000 = 0.104 \text{ kg} (0.229 \text{ lb})$	(7.19)

7.4.2 Abbe–Porro Erecting System

The combination of two Abbe–Porro prisms—air spaced or cemented together side by side with the entrance and exit surfaces facing in opposite directions—creates an image erecting system that functions in the same manner as the Porro erecting system. In the optically equivalent alternate arrangement shown in Figure 7.25, two right-angle prisms are attached with optical cement to the hypotenuse of a Porro prism. This arrangement has the advantage that the largest component (the Porro prism) can be attached to the mechanical surround while the smaller prisms are adequately supported by the cemented joints. As with the Porro erecting system, the Abbe erecting system is not a constant-deviation prism. A design example is given here.

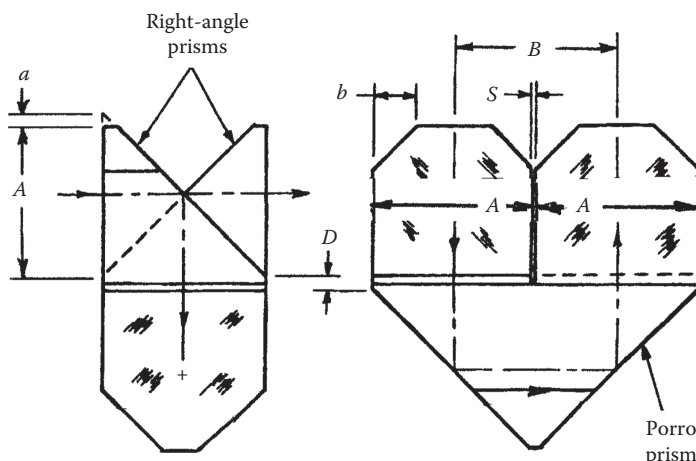
**FIGURE 7.24**

Configuration of a Porro erecting prism system. The interface may be air spaced or cemented.

**DESIGN EXAMPLE 7.15 PORRO ERECTING SYSTEM OF
 $A = 38.100 \text{ mm}$ AND $\rho = 2.510 \text{ g/cm}^3$ (SEE FIGURE 7.24)**

Parameter	Equation Number
$D = 0.100A = 3.810 \text{ mm}$ (0.150 in.)	Chosen value
$t_A = 4.600A = 175.260 \text{ mm}$ (6.900 in.)	(7.65)
$a = 0.100A = 3.810 \text{ mm}$ (0.150 in.)	(7.66)
$B = 1.556A = 59.246 \text{ mm}$ (2.333 in.)	(7.67)
$V = 2.200A^3/1000 = 121.674 \text{ cm}^3$ (7.425 in. ³)*	(7.68)
$W = V\rho/1000 = 0.305 \text{ kg}$ (0.139 lb)*	(7.19)

* Large bevels (dimensions b in Figure 7.24) are here neglected; hence, V and W are overestimated.

**FIGURE 7.25**

Configuration of an Abbe-Porro erecting prism system.

**DESIGN EXAMPLE 7.16 ABBE-PORRO ERECTING SYSTEM
OF $A = 38.100$ mm, AND $\rho = 2.510$ g/cm³ (SEE FIGURE 7.25)**

Parameter	Equation Number
$D = 0.200A = 7.620$ mm (0.300 in.)	Given
$t_A = 4.801A = 162.918$ mm (6.414 in.)	(7.69)
$a = 0.100A = 3.810$ mm (0.150 in.)	(7.66)
$b = 0.358A = 13.658$ mm (0.538 in.)	(7.70)
$S = 0.050A = 1.905$ mm (0.075 in.)	(7.71)
$B = 1.201A + S = 45.758$ mm (1.802 in.)	(7.72)
$V = 3.283A^3/1000 = 181.571$ cm ³ (11.080 in. ³)	(7.73)
$W = V\rho/1000 = 0.534$ kg (0.243 lb)	(7.19)

Note: Large bevels (such as dimension b in Figure 7.25) are neglected; hence, V and W are overestimated.

The Porro and Abbe erecting systems could be alternate design candidates for use in a binocular where an increase in the objective axis separation with respect to the user's interpupillary distance (*IPD*) to enhance stereoscopic vision is usually desirable. From Figure 7.24 and Design Example 7.15, we note that this parameter is $B = 1.556A$ for a Porro system. From Figure 7.25 and Design Example 7.16, the maximum axis separation for an Abbe-Porro erecting system is $B = 1.100A$. For a given aperture $A = 50$ mm and $IPD = 72$ mm, the objective line of sight separation is increased by 25% with the Porro design. This would tend to enhance stereo observation.

Another important design consideration is the ratio of the weights of Porro and Abbe erecting systems for a given aperture A and glass type. Here, a low weight might be favorable. Assuming the same glass to be used in both erecting subassemblies, from the last referenced design examples, we see that the Porro-to-Abbe weight ratio equals the ratio of the volumes or $2.600/3.283 = 0.79$ in favor of the Porro design. Both these comparisons substantiate the nearly unanimous choice of the Porro system for enhanced stereo binocular applications.

7.4.3 Abbe-Koenig Prism

This prism, called the Abbe Type A prism by Kaspereit (1953) and illustrated in Figure 7.26, is made in two parts that typically are cemented together. The larger part has a roof with its dihedral edge parallel to the entering and exiting optical axis. With four reflections, the prism functions as an image erector and frequently is used in binoculars and telescopes of in-line configuration, that is, with coaxial objectives and eyepieces. The figure shows the angles and dimensions of the symmetrical form of this prism that has the same size entrance and exit faces. These faces are perpendicular to the axis so the prism can be used with the input beam collimated or converging. An asymmetrical form with exit face smaller than the entrance face is used in some modern binoculars, such as the Zeiss Victory 8 × 56 model, to reduce weight.

Design Example 7.17 shows equations and dimension calculations for the symmetrical prism system.

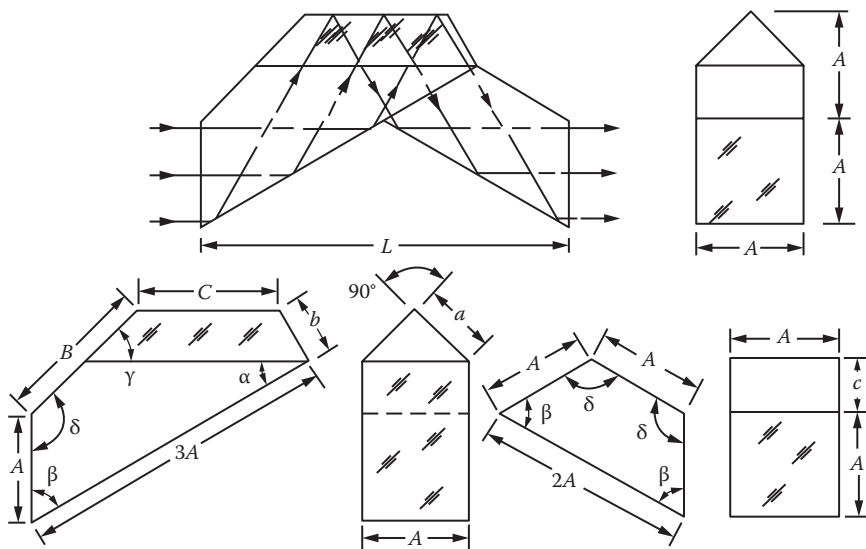


FIGURE 7.26
Configuration of an Abbe-Koenig erecting prism system.

**DESIGN EXAMPLE 7.17 ABBE-KOENIG ERECTING SYSTEM
OF $A = 38.100$ mm AND $\rho = 2.510$ g/cm³ (SEE FIGURE 7.26)**

Parameter	Equation Number
$\alpha = 30^\circ$	Given
$\beta = 60^\circ$	Given
$\gamma = 45^\circ$	Given
$\delta = 135^\circ$	Given
$t_A = 5.196A = 197.968$ mm (7.794 in.)	(7.74)
$a = 0.707A = 26.937$ mm (1.061 in.)	(7.37)
$b = 0.577A = 21.984$ mm (0.866 in.)	(7.75)
$c = 0.500A = 19.050$ mm (0.750 in.)	(7.76)
$B = 1.414A = 53.873$ mm (2.121 in.)	(7.15)
$C = 1.309A = 49.873$ mm (1.964 in.)	(7.77)
$L = 3.464A = 131.978$ mm (5.196 in.)	(7.78)
$V = 3.719A^3/1000 = 205.684$ cm ³ (12.552 in. ³)	(7.79)
$W = V\rho/1000 = 0.516$ kg (1.135 lb)	(7.19)

7.4.4 Roof Schmidt Prism

With four reflections, this prism inverts and reverts the image while deviating the axis by 45°. It is frequently used as the erector system in terrestrial telescopes in which the eye-piece axis is to be tilted upward for ease of access when the line of sight to the object is horizontal (see Figure 7.27). The prism can be used in collimated or converging beams. Its design is summarized in Design Example 7.18.

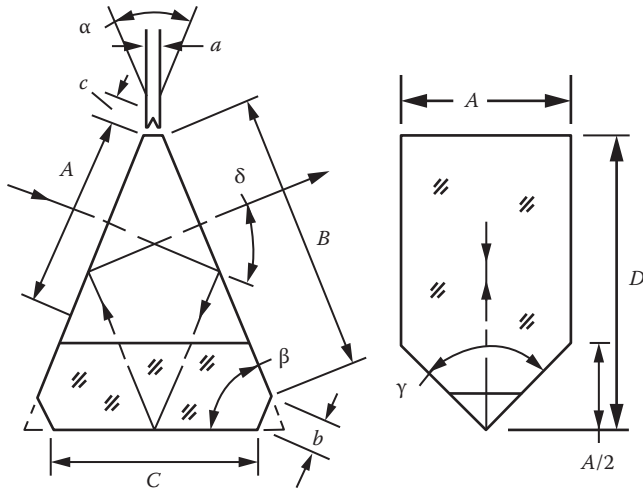
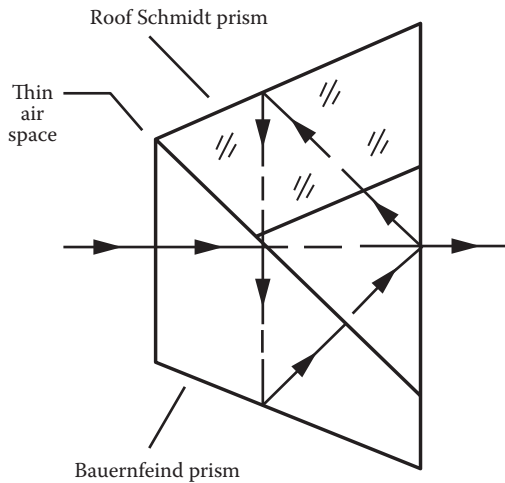


FIGURE 7.27

Configuration of a roof Schmidt erecting prism system.

**DESIGN EXAMPLE 7.18 ROOF SCHMIDT PRISM
WITH $A = 38.100$ mm (SEE FIGURE 7.27)**

Parameter	Equation Number
$\alpha = 45^\circ$	Given
$\beta = 67.5^\circ$	Given
$\gamma = 90^\circ$	Given
$\delta = 45^\circ$	Given
$t_A = 3.045A = 116.015$ mm (4.568 in.)	(7.80)
$a = 0.100A = 3.810$ mm (0.150 in.)	(7.66)
$b = 0.185A = 7.049$ mm (0.278 in.)	(7.81)
$c = 0.131A = 4.991$ mm (0.197 in.)	(7.82)
$B = 1.468A = 55.931$ mm (2.202 in.)	(7.83)
$C = 1.082A = 41.224$ mm (1.623 in.)	(7.84)
$D = 1.527A = 58.179$ mm (2.291 in.)	(7.85)

**FIGURE 7.28**

Combination of a roof Schmidt prism and a 45° Bauernfeind prism to form a *roof Pechan* erecting prism system.

A roof Schmidt prism and a 45° Bauernfeind prism combined as shown in Figure 7.28 forms an axially compact erecting system sometimes called a *roof Pechan* prism because it resembles the classic Pechan design (see Section 7.5.4). The prisms are clamped mechanically or bonded to a common plate (not shown) so as to create a thin air space typically of 0.050–0.100 mm (0.002–0.004 in.) thickness between the diagonal reflecting surfaces. TIR occurs each time the beam reflects from these surfaces, from the roof surfaces, and from the exit face. With the prism's entrance and exit faces perpendicular to the axis, it can be used in the converging beam from an objective lens. To keep the air space clean and free of moisture, a small bead of elastomer or optical cement can be placed around the entire outer edge of the air space and cured in place immediately after the prisms are assembled.

A simpler version of the Schmidt prism does not have a roof so it cannot be used by itself as an image erector. In this design, a simple flat reflecting surface is placed at the location of the dihedral roof edge in Figure 7.27. The bevels, labeled "b" in that figure, usually are retained so the reflecting surface has nominal dimensions of A by C . If combined in series with another prism having a roof, such as an Amici prism, the system will erect the image.

If a Schmidt prism without a roof is coupled with a modified Bauernfeind prism that has a roof with its dihedral edge at the location of the surface labeled "B" in Figure 7.24, another compact in-line erecting system for binoculars or telescopes is created. Seil (1991, 1997) described an application for this type of erecting system. It is shown in Section 8.26 of this volume.

7.4.5 Leman Prism

The Leman image erecting prism (see Figure 7.29) was once popular for use in small binoculars when, as shown in Figure 7.30, a significant increase in objective axis separation relative to the IPD was desired. At maximum IPD, which is typically ~72 mm (2.835 in.), each prism offsets the axis by $3A$ so the maximum objective axis separation is $6A + 72$ mm. Design Example 7.19 provides design equations and sample computations for this type of prism.

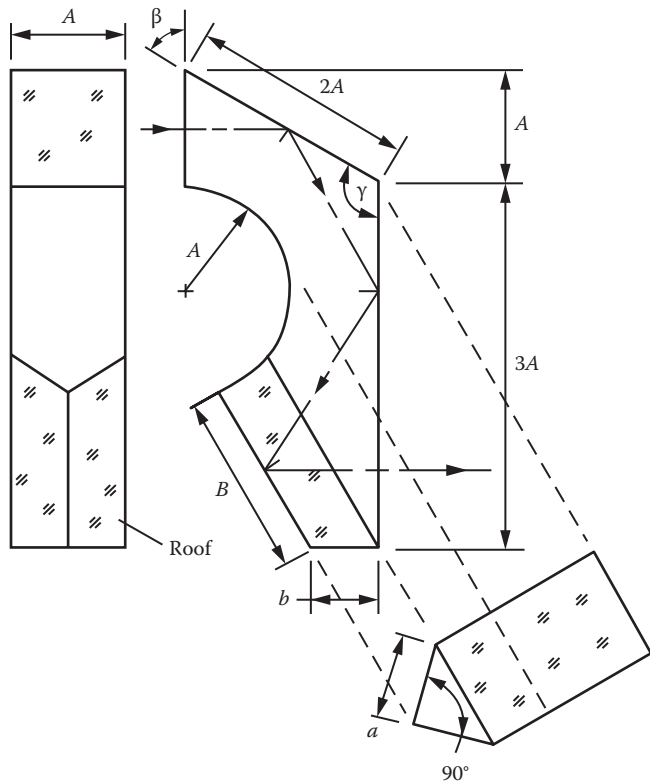
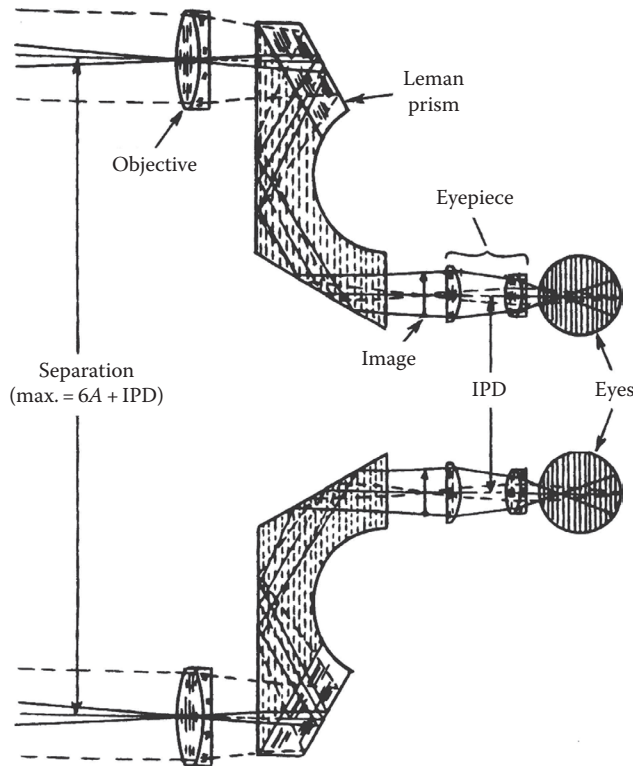


FIGURE 7.29
Configuration of a Leman erecting prism.

**DESIGN EXAMPLE 7.19 LEMAN PRISM WITH
 $A = 20.000 \text{ mm}$ (SEE FIGURE 7.29)**

Parameter	Equation Number
$\alpha = 30^\circ$	Given
$\beta = 60^\circ$	Given
$\gamma = 120^\circ$	Given
$t_A = 5.196A = 197.937 \text{ mm} (5.195 \text{ in.})$	(7.74)
$a = 0.707A = 26.937 \text{ mm} (1.061 \text{ in.})$	(7.37)
$b = 0.577A = 21.984 \text{ mm} (0.866 \text{ in.})$	(7.75)
$B = 1.310A = 49.911 \text{ mm} (1.965 \text{ in.})$	(7.86)

**FIGURE 7.30**

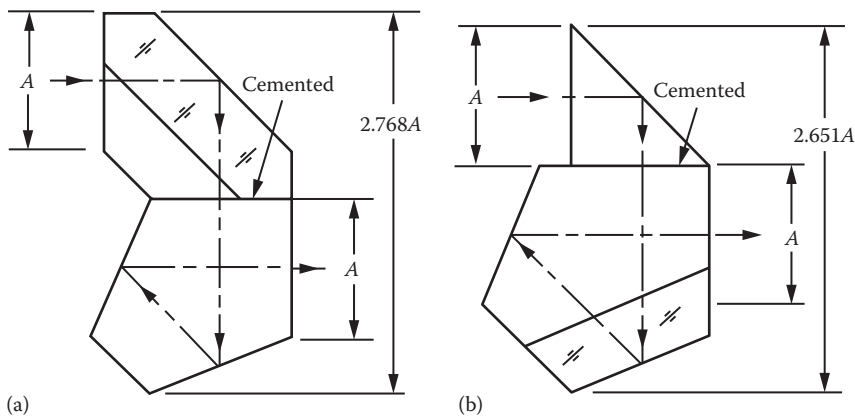
Application of Leman prisms in a binocular. (Adapted from Kaspereit, O.K., *Designing of Optical Systems for Telescopes*, U.S. Army, Washington, DC, 1933.)

7.4.6 Amici/Penta and Right-Angle/Roof Penta Erecting Systems

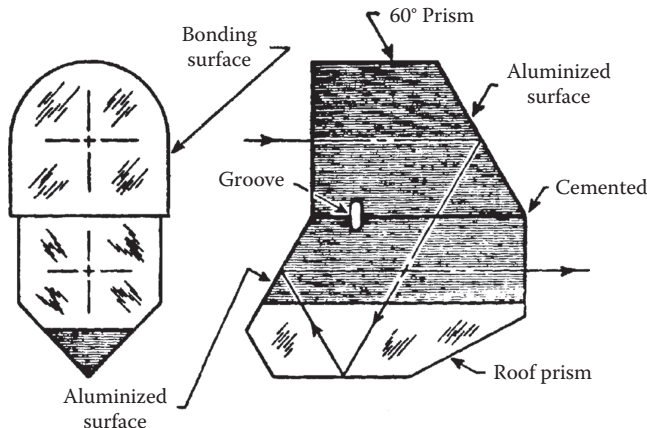
The combination of an Amici prism with a penta prism provides two reflections in each direction perpendicular to the axis, so it can be used as an erecting system. Usually, the prisms are cemented together as illustrated in Figure 7.31a. This design has been used in some binoculars, notably older ones by Hensoldt. A functionally equivalent erecting system uses a right-angle prism and a roof penta prism as shown in Figure 7.31b.

7.4.7 60° Prism/Roof Prism System

A variation of the design represented in Figure 7.31b is illustrated in Figure 7.32. It was used in an experimental pocket-sized military binocular (Yoder, 1960). It was found to be easily manufactured and tested because the roof angle can be accessed at normal incidence before the two prisms are cemented together. TIR occurs at the roof surfaces, but the other reflecting surfaces must be silvered or aluminized. This is also the case with both prisms of Figure 7.31, so the light transmissions of all three subassemblies are essentially equal.

**FIGURE 7.31**

Other erecting prism subassemblies: (a) Amici/penta system and (b) right-angle/roof penta system. (From Yoder, P.R., Jr., *Mounting Optics in Optical Instruments*, 2nd edn., SPIE Press, Bellingham, WA, 2008.)

**FIGURE 7.32**

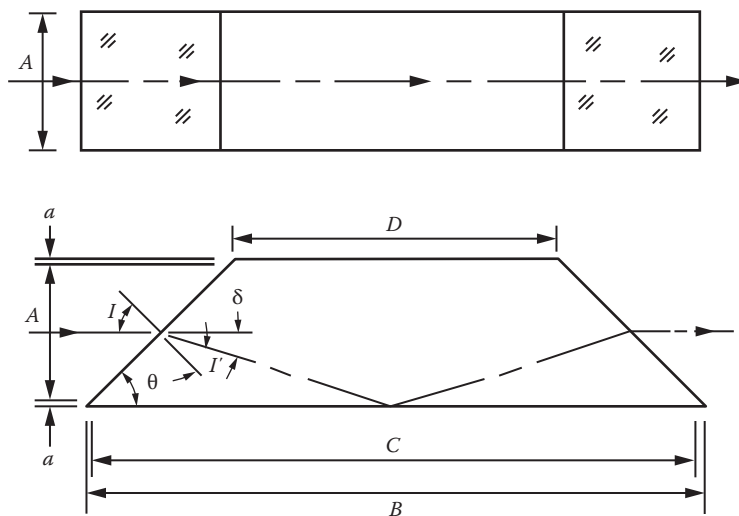
A compact erecting prism assembly used in an experimental military binocular. (From Yoder, P.R., Jr., *J. Opt. Soc. Am.*, 50, 491, 1960.)

7.5 Image-Rotating Prisms

7.5.1 Dove Prism

The Dove prism* is a right-angle prism with the apex section removed. The optical axis enters and exits parallel to the hypotenuse face and at the same height from that surface (see Figure 7.33). This single-reflection prism typically achieves TIR at the hypotenuse face. This and several other types having an odd number of reflections affect the

* Also known as the Harting Dove prism.

**FIGURE 7.33**

Configuration of a Dove image rotator prism.

image orientation only in the plane of reflection. If such a prism is rotated about its optical axis, the image then rotates at twice the speed of the prism. It is most commonly used to counteract the rotation of an image caused by a line of sight scanning motion of other components in an optical system. When used in this manner, the prisms are usually referred to as *derotation* prisms.

Derotation prisms also can be used statically in an optical system that, because of its peculiar configuration of folding mirrors or prisms, would otherwise result in a fixed but undesirably rotated image. The mechanical prism mount must then provide means for achieving the proper orientation of the prism in order to deliver the desired image orientation.

Because of the oblique incidence of the axis at the entrance and exit faces, the Dove prism can be used only in a collimated beam. Alternative versions can have faces tilted at other angles (Sar-El, 1991). Here, we limit consideration to the 45° incidence case because it is the most common. Design Example 7.20 applies to a typical prism.

Some dimensions of the Dove prism depend upon the glass refractive index because of deviations of the optical axis at the tilted faces. Table 7.2 shows how key dimensions of a generic Dove prism vary with changes in refractive index for five Schott glasses.

7.5.2 Double-Dove Prism

The double-Dove prism comprises two Dove prisms, each of aperture $A/2$ by A , with their hypotenuse faces closely air spaced and parallel, resulting in a square aperture. This prism is commonly used as an image rotator or derotator in the same manner as described for the Dove prism. Figure 7.34 shows its configuration while Design Example 7.21 defines a specific design.

For a given aperture, A and index n_d , the double-Dove prism is one-half the length of the corresponding standard Dove prism. To minimize light loss from vignetting, the leading and trailing 45° edges of the double Dove are usually given only minimal protective bevels. This makes those edges fragile, so care must be exercised during manufacture and assembly to avoid damage.

**DESIGN EXAMPLE 7.20 DOVE PRISM OF $A = 38.100$ mm,
 $n_d = 1.517$, AND $\rho = 2.510$ g/cm³ (SEE FIGURE 7.33)**

Parameter	Equation Number
$\theta = 45^\circ$	Given
$I = 45^\circ$	Given
$I' = \arcsin [(\sin I)/n_d] = 27.787^\circ$	(7.87)
$\delta = I - I' = 17.213^\circ$	(7.88)
$a = 0.050A = 1.905$ mm (0.075 in.)	(7.89)
$t_A = [2][(A/2) + a]/\sin \delta = 141.926$ mm (5.588 in.)	(7.90)
$B = (A + 2a)[(1/\tan \delta) + (1/\tan \theta)] = 177.112$ mm (6.973 in.)	(7.91)
$C = B - 2a = 173.302$ mm (6.823 in.)	(7.92)
$D = B - 2(A + a) = 97.102$ mm (3.823 in.)	(7.93)
$V = [(A)(B)(A + 2a) - (A)(A + 2a)^2 - Aa^2]/1000$ $= 215.800$ (13.169 in. ³)	(7.94)
$W = V\rho/1000 = 0.542$ kg (1.192 lb)	(7.19)

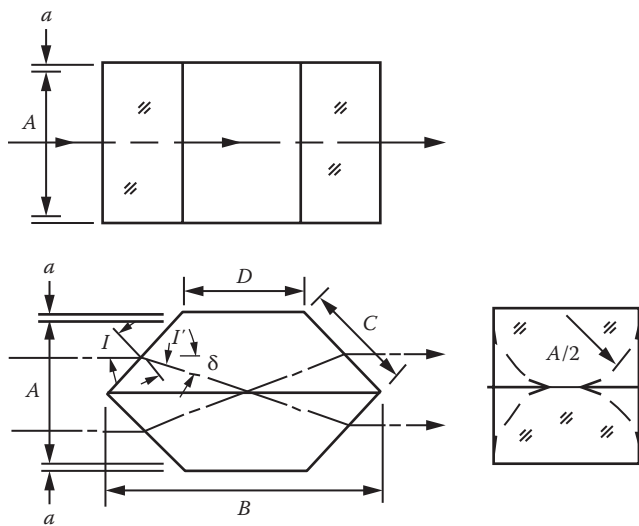
TABLE 7.2

Variations in Dove Prism Dimensions, Volume, and Weight with Glass Type and Refractive Index n_d for Selected Glasses

Glass	NBK7	NSK16	P-LAK35	NSF1	N-LASF9HT
n_d	1.5168	1.6204	1.6935	1.7174	1.8503
ρ (g/cm ³)	2.510	3.580	3.850	3.030	4.410
a (mm)	1.905	1.905	1.905	1.905	1.905
t_A (mm)	141.926	127.906	120.684	118.640	109.366
B (mm)	177.112	162.755	155.083	152.901	142.927
C (mm)	173.302	158.945	151.273	149.091	139.117
D (mm)	97.102	78.935	71.263	69.081	59.107
V (cm ³)	215.800	192.823	180.573	177.090	161.163
W (kg)	0.542	0.690	0.695	0.537	0.711

Note: The prism aperture A is constant at 38.100 mm (1.500 in.).

As shown in the right-hand view of Figure 7.34, a circular beam entering a double-Dove prism is converted into a pair of *D-shaped* beams with curved edges. This tends to reduce the quality of the transmitted image slightly because of diffraction effects. The apertures of optics downstream from the double-Dove prism must be large enough to accept the overall square shape of the converted beam if vignetting is to be avoided. A double image can result if the reflecting surfaces of the prism are not accurately parallel or if the 45° angles are not accurately made.

**FIGURE 7.34**

Configuration of a double-Dove image rotator prism.

**DESIGN EXAMPLE 7.21 DOUBLE-DOVE PRISM OF $A = 38.100$ mm,
 $n_d = 1.517$, AND $\rho = 2.510 \text{ g/cm}^3$ (SEE FIGURE 7.34)**

Parameter

Equation Number

$$\theta = 45^\circ \quad \text{Given}$$

$$I = 45^\circ \quad \text{Given}$$

$$I' = \arcsin [(\sin I)/n_d] = 27.783^\circ \quad (7.1)$$

$$\delta = I - I' = 17.217^\circ \quad (7.88)$$

$$a = 0.050A = 1.905 \text{ mm (0.075 in.)} \quad (7.89)$$

$$t_A = (2)(A/4)/\sin \delta = 64.359 \text{ mm (2.534 in.)} \quad (7.95)$$

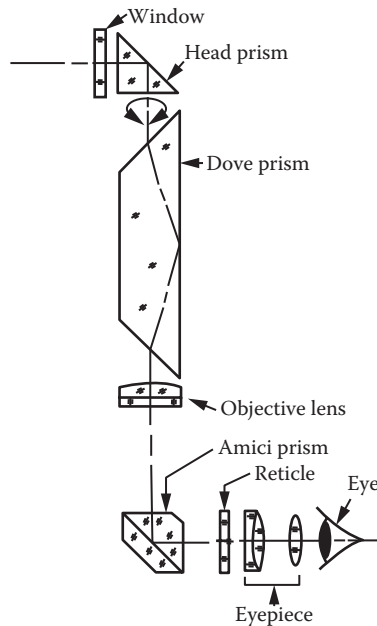
$$B = (A + 2a)[(1/\tan \delta) + (1/\tan \theta)]/2 \\ = 88.578 \text{ mm (3.487 in.)} \quad (7.91)$$

$$C = [(A/2) + a]/\cos \theta = 29.635 \text{ mm (1.167 in.)} \quad (7.96)$$

$$D = B - (A + 2a) = 46.668 \text{ mm (1.837 in.)} \quad (7.97)$$

$$V = (A)(B)(A + 2a) - (2A)[(A/2)^2 + a]^2/1000 \\ = 107.979 \text{ cm}^3 (6.589 \text{ in.}^3) \quad (7.98)$$

$$W = V\rho/1000 = 0.271 \text{ kg (0.596 lb)} \quad (7.19)$$

**FIGURE 7.35**

Application of a Dove image rotator prism in a military panoramic telescope to prevent the rotation of the image as the head prism scans in azimuth.

The most common applications of the Dove and double-Dove prisms are as image derotators. An optical system using a Dove for this purpose is shown in Figure 7.35 and is typical of a military panoramic telescope. The right-angle head prism (or, in some cases, a mirror oriented at 45°) and the window rotate about the vertical axis thereby pointing the line of sight at objects located in various horizontal (or azimuthal) directions. Without the derotator prism, this scanning of the line of sight would rotate the image seen by the user. By turning the derotator in synchronism with the scanning motion and at one-half the rotational rate of that motion, the visual image is always kept erect.

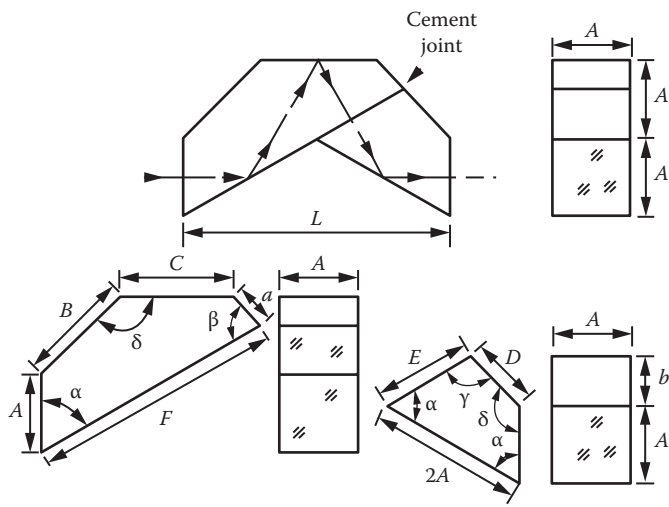
7.5.3 Reversion Prism

Another prism type that can be used as a derotator is the reversion prism described in Kaspereit (1953) (see Figure 7.36). It has two components cemented together and produces three reflections. It resembles the Abbe-Koenig prism but has a single central reflecting surface instead of a roof. It differs from the Dove and double-Dove prisms in that it can be used in a convergent or divergent beam because its entrance and exit faces are normal to the axis. Its central reflecting surface must have a reflecting coating to prevent refraction losses.

Design equations for this prism and parameter calculations for a typical reversion prism are summarized in Design Example 7.22.

7.5.4 Pechan Prism

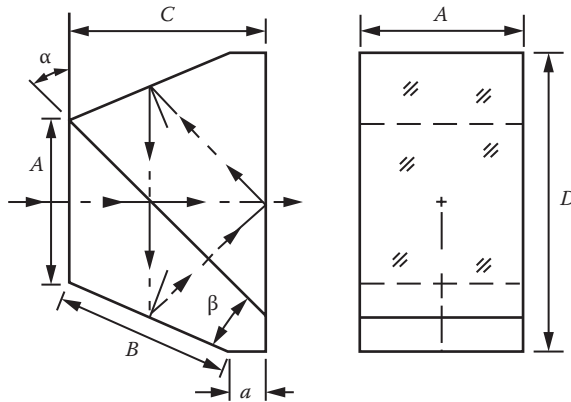
The Pechan prism has five reflections and is frequently used as an axially compact image rotator/derotator in place of the Dove and double-Dove prisms. It can be used in convergent or divergent beams. The design is shown in Figure 7.37. It comprises a Schmidt prism without a roof and a 45° Bauernfeind prism.

**FIGURE 7.36**

Configuration of a reversion prism image rotator. (Adapted from Kaspereit, O.K., *Design of Fire Control Optics ORDM 2-1*, Vol. I, U.S. Army, Washington, DC, 1953.)

**DESIGN EXAMPLE 7.22 REVERSION PRISM OF
 $A = 38.100 \text{ mm}$ AND $\rho = 2.510 \text{ g/cm}^3$ (SEE FIGURE 7.36)**

Parameter	Equation Number
$\alpha = 60^\circ$	Given
$\beta = 60^\circ$	Given
$\gamma = 135^\circ$	Given
$\delta = 135^\circ$	Given
$t_A = 5.196A = 197.968 \text{ mm (7.794 in.)}$	(7.74)
$a = 0.518A = 19.736 \text{ mm (0.777 in.)}$	(7.99)
$b = 0.634A = 24.155 \text{ mm (0.951 in.)}$	(7.100)
$B = 1.414A = 53.873 \text{ mm (2.121 in.)}$	(7.15)
$C = 1.464A = 55.778 \text{ mm (2.196 in.)}$	(7.101)
$D = 0.867A = 33.033 \text{ mm (1.301 in.)}$	(7.102)
$E = 1.268A = 48.311 \text{ mm (1.902 in.)}$	(7.103)
$F = 3.268A = 124.511 \text{ mm (4.902 in.)}$	(7.104)
$L = 3.464A = 131.978 \text{ mm (5.196 in.)}$	(7.78)
$V = 4.196A = 232.065 \text{ cm}^3 (14.162 \text{ in.}^3)$	(7.105)
$W = V\rho/1000 = 0.583 \text{ kg (1.283 lb)}$	(7.19)

**FIGURE 7.37**

Configuration of a Pechan image rotator prism.

Because this prism depends upon TIR at the first and fifth internal reflections, these uncoated surfaces are air spaced by a small separation on the order of 0.050 mm (0.002 in.). Normally, these prisms are held mechanically to provide this space; they cannot be cemented together. The two outer reflecting surfaces (dimensioned B in the figure) must have reflective coatings, such as aluminum or silver. Light transmission suffers relative to some other types of rotation/derotation prisms because of these second-surface reflections and losses at the two uncoated internal surfaces used in transmission by the beam. Design calculations for the Pechan prism are summarized in Design Example 7.23.

**DESIGN EXAMPLE 7.23 PECHAN PRISM OF $A = 38.100$ mm
AND $\rho = 2.510$ g/cm³ (SEE FIGURE 7.37)**

Parameter	Equation Number
$\alpha = 45^\circ$	Given
$\beta = 22.5^\circ$	Given
$A = 38.1$ mm (1.500 in.)	Given
$a = 0.207A = 7.887$ mm (0.310 in.)	(7.106)
$b = 0.100$ mm (0.004 in.)	Assumed
$t_A = 4.621A = 176.060$ mm (6.931 in.)	(7.107)
$B = 1.082A = 41.224$ mm (1.623 in.)	(7.62)
$C = 1.207A = 45.987$ mm (1.810 in.)	(7.108)
$D = 1.707A = 65.037$ mm (2.560 in.)	(7.109)
$V = 1.801A = 99.552$ cm (6.075 in.)	(7.110)
$W = V\rho/1000 = 0.250$ kg (0.550 lb)	(7.19)

7.5.5 Delta Prism

The delta prism is illustrated in Figure 7.38. Its function can be ascertained from the path of the axis depicted in the figure. Three reflections occur so the prism can act as an image rotator or derotator by turning it about the axis of the entering beam. TIR occurs at both the entrance and exit faces that function both in reflection and in transmission. The intermediate (bottom) face is silvered or aluminized to make it reflect. With the proper choice of index of refraction and apex half-angle θ , the internal path can be made symmetrical about the vertical centerline of the prism. The exiting axis is then collinear with the entering axis. Because it has tilted entrance and exit faces, the prism can be used only in a collimated beam.

The design of the delta prism starts with choice of the glass. The index of refraction must be high, typically exceeding 1.700. For practical reasons, we should select values that correspond to an available glass type at the wavelength of interest, such as n_d . Table 7.3 lists six Schott glasses that are possible candidates for use in this type of prism. Similar glasses are made by other optical glass suppliers.

The second step in the delta prism design is to determine the angle θ that, for a given $n_2 = n_d$, causes the entering and exiting axes to be collinear within some small tolerance. Assuming the prism to be in air, these two equations for the angle I'_1 apply:

$$(I'_1) = \arcsin\left(\frac{\sin\theta}{n_2}\right) \quad (7.111)$$

$$(I'_1) = 40^\circ - 90^\circ \quad (7.112)$$

Design Example 7.24 shows how successive approximations can be used to determine the values for θ that makes I'_1 from these equations substantially equal to each other. In this case, agreement between the results from the two equations to <5 arcsec is assumed

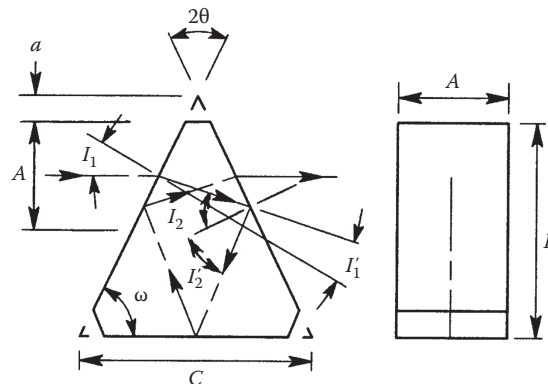


FIGURE 7.38

Configuration of a delta image rotator prism.

TABLE 7.3

Some Schott Glasses with $n_d > 1.700$

Glass	N-SF10	N-SF4	SF11	N-SF6	P-SF68	PLASF50
n_d	1.7283	1.7551	1.7847	1.8052	2.0052	1.8086

DESIGN EXAMPLE 7.24

Part 1: Determination of the Apex Angle for a LaSFN-9 Delta Prism with $n_d = 1.8503$. Assume an error tolerance of 5 arc sec and iterate the apex angle θ until the difference between the results from Equations 7.111 and 7.112 is smaller than that tolerance. The calculations follow.

Trial	θ	I'_r by Equation 7.111 (°)	I'_r by Equation 7.112 (°)	Error (arcsec)
1	26.000	$(0.43837/1.8503) = 13.7048$	$(4)(26.0000) - 90 = 14.0000$	-1063
2	25.900	$(0.43680/1.8503) = 13.6547$	$(4)(25.9000) - 90 = 13.6000$	+197
3	25.920	$(0.43712/1.8503) = 13.6648$	$(4)(25.9200) - 90 = 13.6800$	-55
4	25.918	$(0.43708/1.8503) = 13.6638$	$(4)(25.9180) - 90 = 13.6720$	-30
5	25.916	$(0.43705/1.8503) = 13.6628$	$(4)(25.9160) - 90 = 13.6640$	-4

Note: We iterate until the error between the results is smaller than 5 arcsec (assumed tolerance) (see Figure 7.38).

This final error is acceptable.

Part 2: Check for TIR with the final value from Part 1. How to do this is shown in Design Example 7.25.

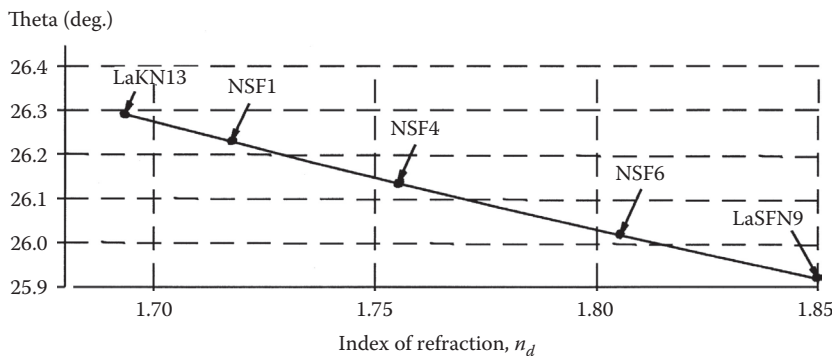


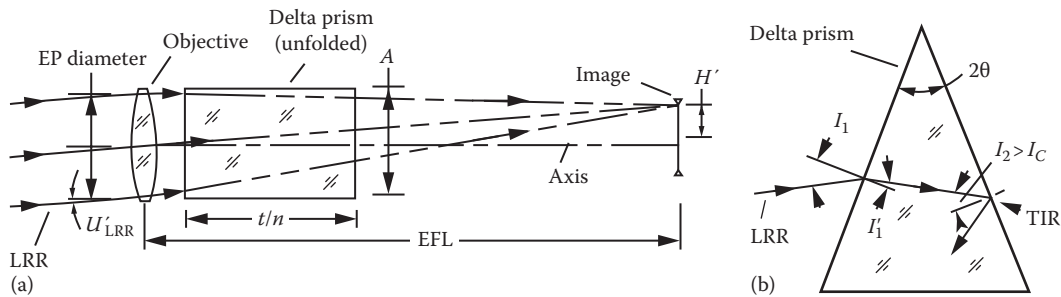
FIGURE 7.39

Variation of the delta prism apex half-angle θ with refractive index.

to be adequate. Schott LaSFN-9 is chosen as the glass. Figure 7.39 shows how θ of the delta prism changes with glass index.

We next determine if all field rays will reflect by TIR inside the delta prism having θ as defined in the last example. This will be true if the lower rim ray (LRR) entering the objective at the bottom of the system's entrance pupil in Figure 7.40a does so because all other field rays will have greater incident angles at the critical second surface of the prism. Note that the prism is depicted as the equivalent glass block of thickness t_A/n so the rays pass through without refraction. The angle U'_{LRR} for the LRR approaching the top of the image is given by

$$U'_{LRR} = \arctan \left\{ \frac{[H' + (EP/2)]}{EFL} \right\} \quad (7.113)$$

**FIGURE 7.40**

(a) Geometry allowing the determination of limiting field ray angle (U'_{LRR}) for TIR in a delta prism. (b) Path of a ray that reflects by TIR in a delta image rotator prism.

From the geometry of Figure 7.40b,

$$I_1 = \theta + U'_{LRR} \quad (7.114)$$

$$I_2 = 2\theta - I'_1 \quad (7.115)$$

By Equation 7.11, $I_C = \arcsin(1/n_2)$. For TIR at the prism's second surface, I_2 must be equal to or greater than I_C .

Design Example 7.25 illustrates the use of these equations to verify TIR for a typical delta prism with high index and apex angle derived as explained earlier. Dimensions for that prism are given a specific aperture and are calculated in Design Example 7.26.

DESIGN EXAMPLE 7.25 VERIFICATION OF TIR FOR ALL FIELD RAYS PASSING THROUGH A DELTA PRISM (SEE FIGURE 7.40a)

The system shown in Figure 7.40a represents a 7×35 telescope with a total field in object space of 7° . The objective EFL is 175 mm (6.890 in.). The LRR enters at the maximum semi-field angle of 3.5° directed toward the top of the image at a height $H' = (\text{EFL})(\tan 3.5^\circ) = 10.703$ mm (0.421 in.). The LRR angle to the axis approaching the image is given by

$$U_{LRR} = \arctan = \frac{\frac{\text{EP}}{2} + H'}{\text{EFL}}.$$

In Figure 7.40b, the prism apex angle 2θ is that derived in the last example (51.832°) for n of 1.8503. The angle $I_1 = \theta + U'_{LRR} = 25.916^\circ + \arctan \{ [10.703 + (35.000/2)] / 175.000 \} = 35.071^\circ$. By Equation 7.11, $I'_1 = \arcsin(\sin 35.071 / 1.8503) = 18.092^\circ$. By the geometry of Figure 7.40b, $I_2 = (2)(25.916) - 18.092 = 33.740^\circ$.

For TIR to occur, I_2 must equal or exceed $I_C = \arcsin(1/n_2) = 32.7145^\circ$ per Equation 7.11. In this design, I_2 for the LRR of concern is greater than I_C so it will reflect by TIR. All other rays within the binocular field of view also will reflect by TIR because they are incident on the prism's reflecting surface at angles of incidence greater than that of the LRR.

DESIGN EXAMPLE 7.26 GEOMETRIC DESIGN OF A DELTA PRISM WITH $A = 34.000 \text{ mm}$ (1.339 in.), $n = 1.8503$, $\theta = 25.916^\circ$, AND $\rho = 4.440 \text{ g/cm}^3$ (SEE FIGURE 7.38)

Parameter	Equation Number
$\omega = 90^\circ - \theta = 90^\circ - 25.916^\circ = 64.084^\circ$	(7.114)
$a = 0.100A = 3.400 \text{ mm}$ (0.134 in.)	(7.66)
$B = 1.483A = 50.427 \text{ mm}$ (1.986 in.)	(7.117)
$C = 2.414A = 82.062 \text{ mm}$ (3.231 in.)	(7.118)
$t_1 = 0.667A = 22.685 \text{ mm}$ (0.893 in.)	(7.119)
$t_2 = 0.824A = 28.033 \text{ mm}$ (1.104 in.)	(7.120)
$t_A = 2.982A = 101.427 \text{ mm}$ (3.993 in.)	(7.121)
$V = 1.503A^3 = 59.074 \text{ cm}^3$ (3.608 in. ³)	(7.122)
$W = V\rho/1000 = 0.262 \text{ kg}$ (0.119 lb)	(7.19)

7.6 Other Prism Types

7.6.1 Internally Reflecting Axicon Prism

Some axicons have a conical refracting surface and a coated flat reflecting surface to return the beam to and through the conical surface in the reverse direction. One such configuration is shown in Figure 7.41. Its design equations are given in Design Example 7.27.

A typical application is to change a small circular laser beam into an annular beam with a larger outside diameter (OD) (see, e.g., Yoder et al., 1975).

Because of its rotational symmetry, the axicon is made with a circular cross section and is usually mounted within an elastomeric ring inside a cylindrical mount. The apex is

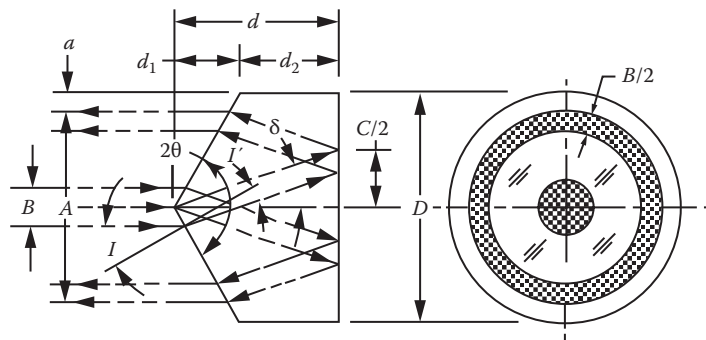


FIGURE 7.41

Configuration of an internally reflecting axicon prism. (From Yoder, P.R. et al., *Appl. Opt.*, 14, 1890, 1975.)

**DESIGN EXAMPLE 7.27 INTERNALLY REFLECTING AXICON PRISM
OF REFRACTIVE INDEX $n = 1.517$ AND $\rho = 2.51 \text{ g/cm}^3 = 0.091 \text{ lb/m}^{-3}$**

Parameter	Equation Number
$A = \text{Output annulus outside diameter (OD)} = 38.100 \text{ mm (1.500 in.)}$	Given
$B = \text{Input beam OD} = 3.000 \text{ mm (0.118 in.)}$	Given
$\theta = 60^\circ$	Given
$I_1 = 90^\circ - \theta = 30^\circ$	(7.123)
$I'_1 = \arcsin(\sin I_1/n) = 19.247^\circ$	(7.1)
$\delta = I_1 - I'_1 = 10.753^\circ$	(7.124)
$a = 0.100A = 3.810 \text{ mm (0.150 in.)}$	(7.66)
$D = A + 2a = 45.720 \text{ mm (1.800 in.)}$	(7.125)
$r = D/2 = 22.860 \text{ mm (0.900 in.)}$	(7.126)
$d_1 = [(A/2) + a]/\theta \tan \theta = 13.198 \text{ mm (0.520 in.)}$	(7.127)
$d = (A/4) [(1/\tan \theta) + (1/\tan \delta)] = 55.642 \text{ mm (2.191 in.)}$	(7.128)
$d_2 = d - d_1 = 42.444 \text{ mm (1.671 in.)}$	(7.129)
$C = 2d \tan \delta = 21.139 \text{ mm (0.832 in.)}$	(7.130)
$t_A = A/(2\sin \delta) = 102.079 \text{ mm (4.019 in.)}$	(7.131)
$V = (\pi r^2/1000)[(d_1/3) + d_2] = 76.917 \text{ cm}^3 (4.693 \text{ in.}^3)$	(7.132)
$W = V\rho/1000 = (76.917)(2.51)/1000 = 0.1943 \text{ kg (0.427 lb)}$	(7.19)

either a sharp point or carries only a very small protective bevel. A centrally perforated flat mirror inclined at 45° to the axis located between input laser and the axicon provides a convenient way to separate the coaxial beams.

An in-line refracting version of this reflecting axicon with identical conical surfaces at either end has been used to accomplish the same function as described here, but without the reversal of beam direction at the flat surface. It is twice as long and is more expensive to fabricate because of the additional conical surface.

7.6.2 Cube-Corner Prism

A corner cut symmetrically and diagonally from a solid glass cube and having all four surfaces subsequently polished flat and at precise 90° angles to each other creates a prism in the geometrical form of a tetrahedron (four-sided polyhedron) (see Figure 7.42). Such a prism has been referred to by various authors as a *corner cube** or a *tetrahedral prism*. Light entering the largest face reflects internally in sequence from the other three faces and exits through the entrance face. TIR occurs at each internal surface for commonly used refractive index values. The return beam contains six segments, one from each of the triangular shaped areas within the circular frontal aperture indicated by the inscribed circle.

* This is a common, but not precise name for the *cube-corner* prism.

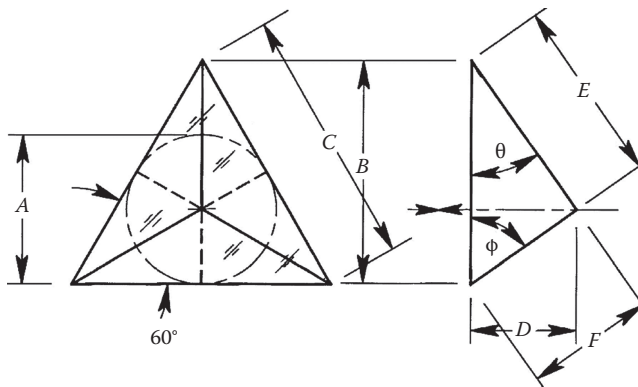


FIGURE 7.42
Design configuration of a retrodirective cube-corner prism.

A perfect cube-corner prism is perfectly retrodirective. The relationships between inaccuracies of the 90° dihedral angles and the errors in parallelism between the various exiting beams and the entering beam have been explained by Yoder (1958) and others. In brief, if we let the prism's angles each have an error equaling a tolerance of ϵ , the resulting return beam deviations $\delta_{1,2,3}$, $\delta_{2,3,1}$, $\delta_{3,1,2}$ are as listed in Table 7.4. These reflected beams diverge as they return toward the source of the entering beam. The term n is the refractive index of the glass. Note that only three δ values are needed for each case because, for example, the reflection sequence from surfaces 1-2-3 produces the same result as for sequence 3-2-1.

Figure 7.43 shows a graphical representation of the six images returned by a perfect and five imperfect cube-corner prisms drawn to an arbitrary but constant scale. The separations and relative orientations of the spots correspond to the angular values listed in Table 7.4. Closely adjacent spots indicate that multiple beams are superimposed at the centers of those angular locations. The angular errors in parallelism between the input beam axis and those of the reflected beams are indicated for Case 6 by the arrow. Similar interpretations can be applied to the other cases.

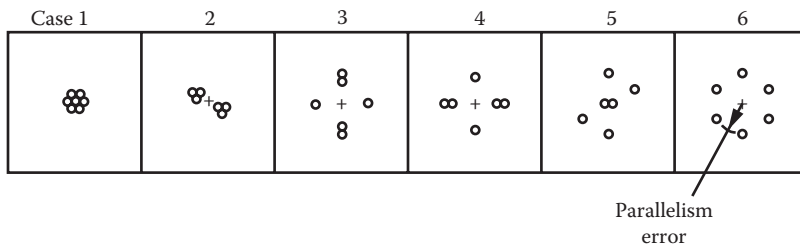
Design Example 7.28 shows design equations for a triangular faced cube-corner prism of aperture A . The retrodirective feature of the cube-corner prism is used to advantage

TABLE 7.4

Parallelism Errors Resulting from Errors in 90° Dihedral Angles

Case No.	1	2	3	4	5
Surf. 1-2	$\pm\epsilon$	$\pm\epsilon$	$\pm\epsilon$	$\pm\epsilon$	$\pm\epsilon$
Surf. 1-3	Zero	$\pm\epsilon$	$\pm\epsilon$	$\pm\epsilon$	$\pm\epsilon$
Surf. 2-3	Zero	Zero	Zero	$\pm\epsilon$	$\pm\epsilon$
$\sin \delta_{1,2,3}$	$2n\sqrt{2} \sin \epsilon / \sqrt{3}$	$2n\sqrt{2} \sin \epsilon$	$2n\sqrt{2} \sin \epsilon / \sqrt{3}$	$4n\sqrt{2} \sin \epsilon / \sqrt{3}$	$4n\sqrt{2} \sin \epsilon / \sqrt{3}$
$\sin \delta_{2,3,1}$	$2n\sqrt{2} \sin \epsilon / \sqrt{3}$	$2n\sqrt{2} \sin \epsilon$	$2n\sqrt{2} \sin \epsilon / \sqrt{3}$	$4n\sqrt{2} \sin \epsilon / \sqrt{3}$	$4n\sqrt{2} \sin \epsilon / \sqrt{3}$
$\sin \delta_{3,1,2}$	$2n\sqrt{2} \sin \epsilon / \sqrt{3}$	$2n\sqrt{2} \sin \epsilon / \sqrt{3}$	$2n\sqrt{2} \sin \epsilon$	Zero	$4n\sqrt{2} \sin \epsilon / \sqrt{3}$
$\delta_{1,2,3}$	$1.63n\epsilon$	$2.83n\epsilon$	$1.63n\epsilon$	$3.26n\epsilon$	$3.26n\epsilon$
$\delta_{2,3,1}$	$1.63n\epsilon$	$2.83n\epsilon$	$1.63n\epsilon$	$3.26n\epsilon$	$3.26n\epsilon$
$\delta_{3,1,2}$	$1.63n\epsilon$	$1.63n\epsilon$	$2.83n\epsilon$	Zero	$3.26n\epsilon$

Source: Adapted from Yoder, P.R., Jr., *J. Opt. Soc. Am.*, 48, 496, 1958.

**FIGURE 7.43**

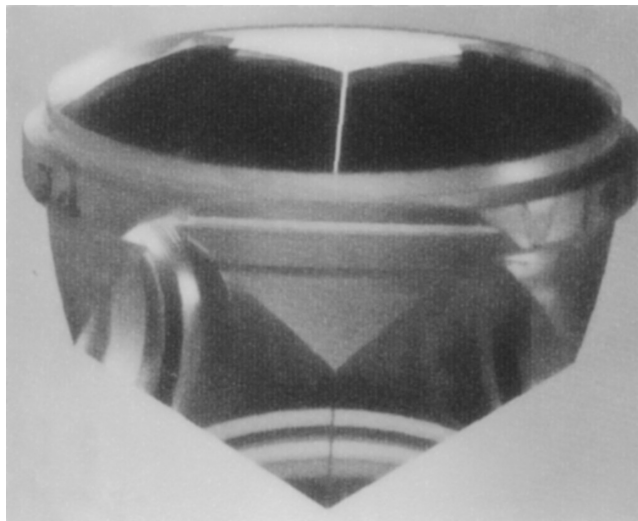
Representation of return beam parallelism errors resulting from uniform dihedral angle errors as listed in Table 7.4. (From Yoder, P.R., *J. Opt. Soc Am.*, 48, 496, 1958.)

DESIGN EXAMPLE 7.28 CUBE-CORNER PRISM OF APERTURE A = 38.100 mm (1.500 in.)

Parameter	Equation Number
$\theta = 35.264^\circ$	Given
$\varphi = 54.736^\circ$	Given
$B = [(A/2)/\sin 30^\circ] + (A/2) = 1.500A = 57.150 \text{ mm (2.250 in.)}$	(7.133)
$C = A/\tan 30^\circ = 1.732A = 65.989 \text{ mm (2.598 in.)}$	(7.134)
$D = \text{Atan } \theta = 0.707A = 26.937 \text{ mm (1.060 in.)}$	(7.135)
$E = B \sin \theta = 0.866A = 32.995 \text{ mm (1.229 in.)}$	(7.136)
$F = E/\tan \theta = 1.225A = 46.673 \text{ mm (1.838 in.)}$	(7.137)
$t_A = 2D = 1.414A = 53.873 \text{ mm (2.121 in.)}$	(7.138)

in such applications as interferometry, laser tracking of cooperative targets, or those involving spatially adjacent or coaxial transmitter and receiver optical systems used for very long range operation such as from the Earth to a spacecraft or to the Moon. During the beam's transit time from the source to the target and return, transverse orbital motion may cause the return beam to miss the receiver. By introducing divergence to the return beams, it may be that enough return energy can be collected to accomplish the mission.

The cube-corner prism shown in Figure 7.41 and defined in Design Example 7.28 has a triangular form with sharp dihedral edges. The most popular variation of this design has its rim ground to a circular shape circumscribing the aperture (the dashed line). Figure 7.44 shows an example. This is one of the 426 fused silica prisms used on the laser geodynamic satellite (LAGEOS) launched to the Moon by NASA in 1976 to provide scientists with extremely accurate measurements of movements of the Earth's crust as a possible aid to understanding earthquakes, continental movement, and polar motion. The dihedral angles of the prisms were each accurately 1.25 arcsec greater than 90°. A laser beam transmitted to the satellite was returned as six beams with sufficient divergence (from the aforementioned theory, $3.26 \times 1.46 \times 1.25 = 5.95 \text{ arcsec}$) for some

**FIGURE 7.44**

A precision fused silica cube-corner prism with a 3.81 cm (1.50 in.) circular aperture. (Courtesy of Goodrich Corp., Danbury, CT.)

energy to reach a receiver telescope on Earth even though the Moon moved significantly relative to the Earth during the beam's round-trip transit time.

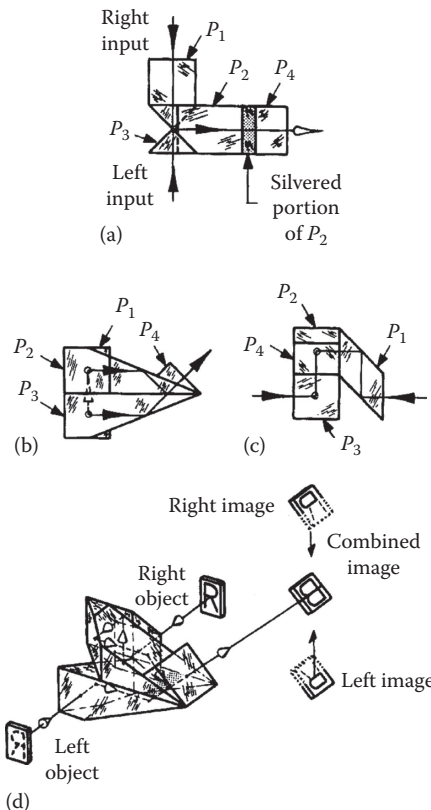
Another cube-corner prism configuration has the rim cut to a hexagonal shape tangent to the prism's circular clear aperture. This allows several of the prisms to be tightly grouped together to form a mosaic of closely packed retrodirective prisms, thereby increasing the effective aperture of the group. These are frequently used as targets for surveying purposes.

Mirror versions of the cube-corner prism are frequently used when operation outside the transmission range of normal refracting materials is needed. This so-called *hollow cube-corner* (HCR) or *triple mirror* generally has reduced weight as compared with a solid prism version for a given aperture. The deviation versus angle error relationships cited earlier also pertain to the mirror version except that n reduces to unity. Several types of HCRs designed for a variety of applications and having different mechanical configurations are described in Section 9.6 of this volume.

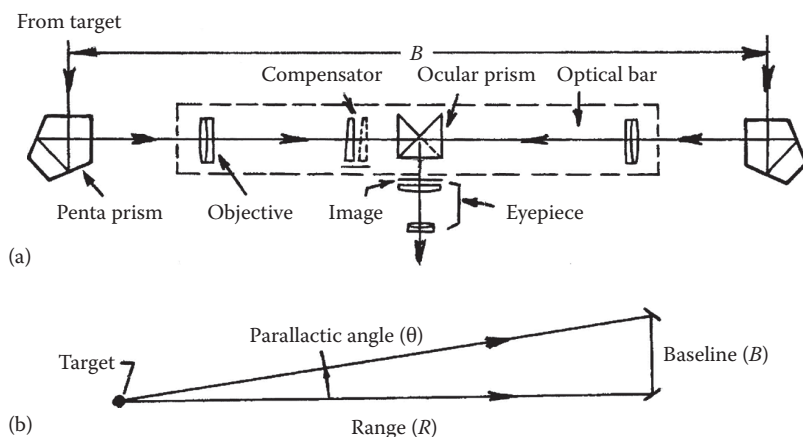
7.6.3 Ocular Prism for a Coincidence Range Finder

The prism subassembly shown in Figure 7.45 was designed and made by Carl Zeiss for use in a military split-field coincidence-type optical range finder. In order to facilitate explanation of its design, we first describe the function of this type of range finder.

As indicated schematically in Figure 7.46a, light beams from a distant target enter the range finder through windows (not shown) at either end of the instrument and are folded toward the center of the device by penta prisms. Images formed by the two objective lenses are combined by the ocular prism and viewed through an eyepiece. Because the target is at a finite distance, the beams forming the images are very slightly inclined with respect to each other and the images are not coincident. The operator deflects the image coming from one side of the instrument by moving an adjustable compensator (shown in view [a] as a longitudinally sliding wedge [see Section 7.6.6.3 of this volume]) so that it appears superimposed upon the image from the other side of the instrument.

**FIGURE 7.45**

An ocular prism designed by Zeiss for a coincidence-type optical range finder: (a) top view, (b) side view, (c) end view, and (d) isometric view. (Adapted from MIL-HDBK-141, *Optical Design*, Defense Supply Agency, Washington, DC, 1962.)

**FIGURE 7.46**

(a) Optical schematic of a typical coincidence-type optical range finder. (b) The range triangle showing parameters used to determine the range to a target. (Adapted from Kaspereit, O.K., *Designing of Optical Systems for Telescopes*, U.S. Army, Washington, DC, 1933.)

By reading a scale connected to the movable wedge, the parallactic angle θ is measured and range R to the target is calculated from this equation:

$$R = \frac{B}{\tan \theta} \quad (7.139)$$

where the optical baseline B is the lateral separation of the beam centerlines entering the range finder and θ the small angle of divergence between the axes of the two input light beams from the target (see Patrick, 1969).

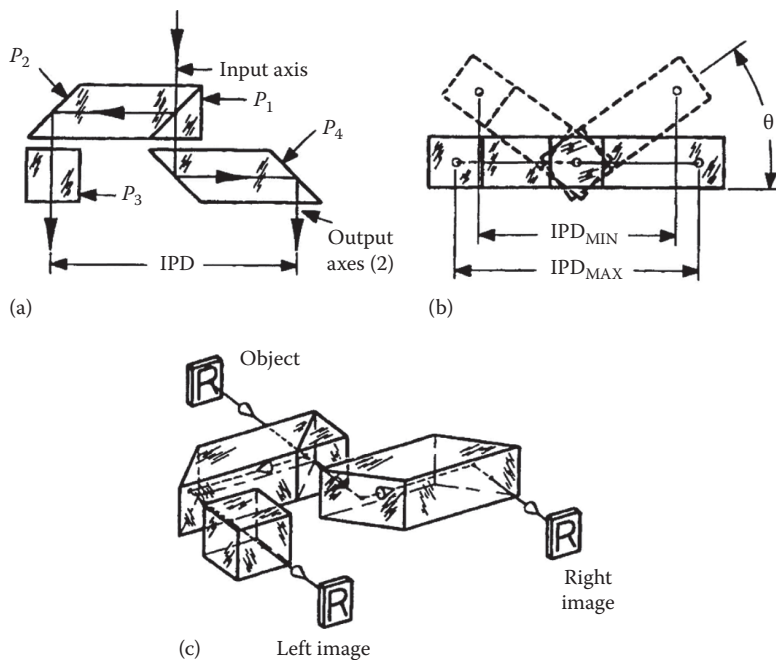
The optics within the dashed rectangle of view (a) in Figure 7.46 are all mounted on a rigid structure called the *optical bar* in order to maintain precise alignment to each other. This structure is usually made of material (such as glass, fused silica, or Invar) with low CTE to maximize thermal stability. Because of their inherent insensitivity to rotation in the plane of the figure, the penta prisms need not be attached to the bar. Rotation of either penta prism in a plane perpendicular to that of the figure will move its image relative to the other in the vertical direction. A mechanism, sometimes called the *halving adjustment* and which allows the operator to adjust the vertical position of one image, may be built into the optical system. A plane-parallel glass plate nominally perpendicular to the optic axis but capable of slight rotation about a horizontal axis is commonly used. Small changes in the plate's tilt move the following image vertically without affecting image quality.

The particular ocular prism design depicted in Figure 7.45 comprises four prism elements, designated P_1 through P_4 , cemented together. The refracting angles of P_2 , P_3 , and P_4 are all 22.5° , and the eyepiece axis is inclined upward at 45° . The beam from the right objective enters the rhomboid prism P_1 and, after five internal reflections in P_1 and P_2 , passes through P_4 and focuses at the image plane. The last reflection in this path is at a silvered area on a portion of the bottom surface of P_2 , so this beam forms the top half of the image. The beam from the left objective reflects twice inside P_3 and passes through P_4 to the image plane. This beam misses the silvered area on P_2 and forms the bottom half of the image. The fact that the observed image is divided vertically into two parts coming through different optical systems leads to the designation of this range finder as a split-field, coincidence-type instrument. The operator sees the two half images misaligned laterally until he adjusts the compensator to bring one image directly over the other image. This establishes coincidence and allows the range to be determined from the calibrated range scale.

Several other versions of ocular prisms for range finders are described by Kaspereit (1953) and MIL-HDBK-141 (1962). All function in the same general manner as just described, that is, they combine the images produced by the left and right optical systems so that the angle θ can be measured and the range calculated.

7.6.4 Biocular Prism System

The prism system shown in Figure 7.46 can be used in telescopes and microscopes when both eyes are to observe the same image as presented by a single objective. It does not provide stereoscopic vision and is hence called *biocular* rather than *binocular*. From view (a), it can be seen to consist of four prisms: a right-angle prism, P_1 , cemented to a rhomboid prism, P_2 , with a partially reflective (beam splitting) coating at the cemented interface; an optical path equalizing block, P_3 ; and a second rhomboid prism, P_4 . The observer's IPD is designated as *IPD*. By rotating the prisms symmetrically about the input axis, the IPD is changed to suit the individual using the instrument. Typically, the IPD is adjustable from

**FIGURE 7.47**

A beam splitting biocular prism system: (a) top view, (b) end view, and (c) isometric view. IPD is the interpupillary distance. (Adapted from MIL-HDBK-141, *Optical Design*, Defense Supply Agency, Washington, DC, 1962.)

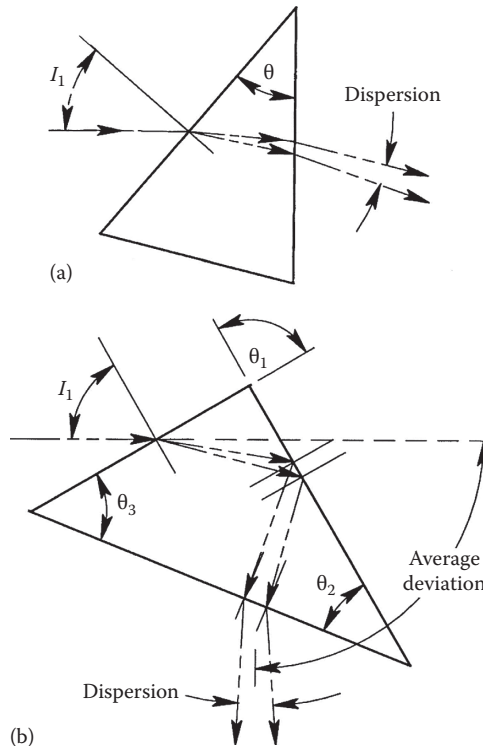
at least 56 to 72 mm (2.20 to 2.83 in.). An external scale usually is provided on the optical instrument to allow easy reference for setting this distance.

Applications of this type of prism assembly include optical microscopes and military night vision devices utilizing image intensifiers.

7.6.5 Dispersing Prisms

Prisms are frequently used to separate, that is, disperse, polychromatic light beams into their constituent colors in instruments such as spectrometers and monochromators. The index of refraction n of the optical material varies with wavelength, so the deviation (measured with respect to the initial incident ray direction) of any ray transmitted at other than normal incidence to the prism's entrance and exit surfaces will depend upon n , the angle of incidence at the entrance face, and the prism's apex angle, θ .

Figure 7.48 illustrates two typical dispersing prisms. In each case, a single ray of *white* light is incident at angle I_1 . Inside each prism, this ray splits into a spectrum of variously colored rays. For clarity, the angles between rays are exaggerated in the figures. After refraction at the exit faces, rays of blue, yellow, and red wavelengths emerge with different deviation angles δ_λ . The blue ray is deviated the most because n_{BLUE} is greater than n_{RED} . If the emerging rays are imaged onto film, a detector array, or a screen by a lens or mirror, a multiplicity of images of different colors will be formed at slightly different transverse locations. Although we refer here to colors such as blue, yellow, and red, it should be understood that the phenomenon of dispersion applies to all wavelengths, so we really mean the shorter, intermediate, and longer wavelength radiation under consideration in any given application.

**FIGURE 7.48**

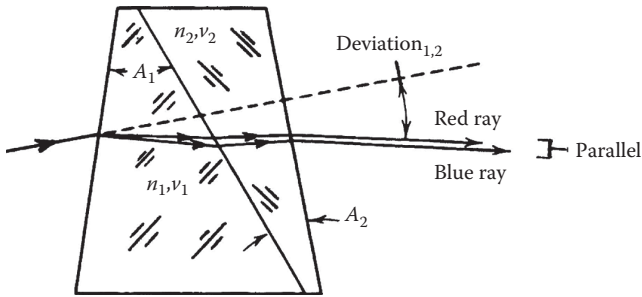
Dispersion of white light by (a) a simple prism and (b) a constant-deviation prism involving TIR. (From Yoder, PR., Jr., *Mounting Optics in Optical Instruments*, 2nd edn., SPIE Press, Bellingham, WA, 2008.)

In the simpler prism design shown in Figure 7.48a, only refraction occurs. In Figure 7.48b that has one reflection as well as refraction, the deviation is unchanged for small rotations of the prism about an axis perpendicular to the plane of refraction; hence, the prism is designated as *constant deviation*. The refractive index in this case usually is chosen to be large enough to cause TIR to occur at the reflecting surface, because this enhances light transmission.

If a collimated beam of light of wavelength λ passes symmetrically through a prism so that $I_1 = -I'_1$ and $I'_1 = -I_1$, the deviation of the prism for that wavelength is a minimum and $\delta_{\text{MIN}} = 2I_1 - \theta$. This condition is the basis of one means for experimental measurement of the index of refraction of a transparent medium in which the minimum deviation angle, δ_{MIN} , of a prism made of that material is found by successive approximations. The following equation is then applied:

$$n_{\text{PRISM}} = \frac{\sin[(\theta + \delta)/2]}{\sin(\theta/2)} \quad (7.140)$$

If we want any two of the various colored rays to emerge from the prism parallel to each other, we must use a combination of at least two prisms made of different glasses. Usually, these prisms are cemented together. Such a prism is called an *achromatic prism*. Figure 7.49 shows one configuration for an achromatic prism. All such prisms can be designed by choosing refractive indices and the first prism's apex angle and then

**FIGURE 7.49**

A typical achromatic dispersing prism. (From Smith, W.J., *Modern Optical Engineering*, 4th edn., McGraw-Hill, New York, 2008.)

repeatedly applying Snell's law to find the appropriate incident angle and second prism apex angle that gives the desired deviation for a chosen wavelength and the desired dispersion for two other wavelengths that bracket the chosen one. The angle between the exiting rays with the shortest and longest wavelengths is called the *primary chromatic aberration*; here, it should be essentially zero. The angle between either of these extreme wavelength rays and that with an intermediate wavelength is called *secondary chromatic aberration* of the prism.

The design of an achromatic prism of the type shown in Figure 7.49 might well proceed as follows. We first choose the glasses to try in the design. We then might assume that the yellow ray enters the first prism at minimum deviation in air. For any assumed value for θ , the angles $I'_1 = I_2 = \theta/2$ for that ray. The red and blue rays would, of course, be dispersed. We use Snell's law (Equation 7.1) to find angle I_1 for the yellow (sodium d) ray. We then add the second prism and redetermine angle I'_2 . Finally, we calculate the required angle θ_2 from

$$\cotan \theta_2 = - \frac{\Delta n_2}{2\Delta n_1 \sin(\theta_1/2) \cos I'_2} + \tan I'_2 \quad (7.141)$$

where Δn_1 and Δn_2 are the index differences for the red and blue wavelengths in prisms 1 and 2.

To complete the first-order design of a dispersing prism requires the calculation of the required apertures. Usually, we assume a collimated input beam and make the apertures of the prism large enough to not vignette any of the dispersed beams.

7.6.6 Thin Wedge Prisms

7.6.6.1 Thin Wedge

Prisms with small geometric apex angles and axial thicknesses that are small compared with the component apertures are called *optical wedges*. A typical configuration is shown in Figure 7.50. Because the apex angle is small, we can assume that the angle expressed in radians equals its sine, and, rewriting Equation 7.146, we obtain the following simple equation for the wedge deviation in air:

$$\delta_\lambda = (n_\lambda - 1)\theta \quad (7.142)$$

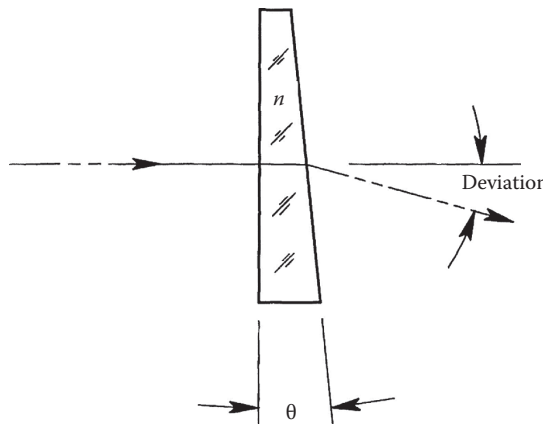


FIGURE 7.50
Deviation of a ray by a thin optical wedge.

Another important equation expresses the dispersion, that is, the chromatic aberration, of the wedge as

$$d\delta_\lambda = dn_\lambda \theta \quad (7.143)$$

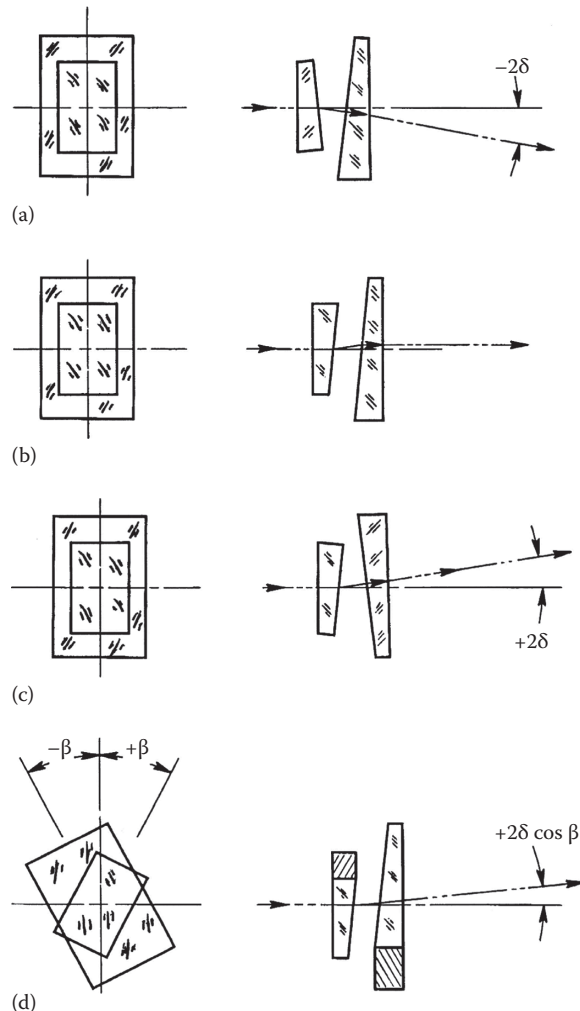
A wedge designed with these equations is one providing minimum deviation. A common arrangement in optical instruments has the incident beam normal to the entrance face. Then $I_2 = \theta$, $I'_2 = \arcsin(ns \sin I_2)$, and $\delta = I'_2 - \theta$. If not otherwise specified, we would assume n to apply to the center wavelength of the spectral bandwidth of interest. The deviation angle will differ only very slightly from that given by Equation 7.95.

7.6.6.2 Risley Wedge System

Two identical thin optical wedges mounted in series and rotated equally in opposite directions about the optical axis form an adjustable wedge. They are used in various applications, such as to provide variable pointing of laser beams, to angularly align the axis of one portion of an optical system to that of another portion of that system, to test ocular convergence in ophthalmology, or to measure distance in some optical range finders. They are referred to as Risley wedges or as a diasporometer, the latter term most frequently associated with their use in range finders.

The action of a Risley wedge system is shown in Figure 7.51. Usually, the wedges are circular in shape; here, their apertures are shown (on left) as small and large rectangles for clarity. In views (a) and (c), the wedges are shown in their two positions for maximum deviation. The apexes are adjacent and the deviation $\delta_{SYSTEM} = 2\delta$, where δ is the deviation of one wedge. If the wedges are turned from either maximum deviation position in opposite directions by β (see Figure 7.51d), the deviation becomes $\delta_{SYSTEM} = 2\delta \cos \beta$ and the change in deviation from the maximum achievable value is $2\delta(1 - 2\cos \beta)$. If we continue to turn the wedges until $\beta = 90^\circ$, we obtain the condition shown in Figure 7.51b, where the apexes are opposite, the system acts as a plane-parallel plate, and the deviation is zero.

Since counterrotation of the wedges in a Risley wedge system provides variable deviation in one axis, a second such system, usually identical to the first, is sometimes added in series with the first to provide independent deviations in orthogonal directions. The deviations from the two systems add vectorially in a rectangular coordinate system.

**FIGURE 7.51**

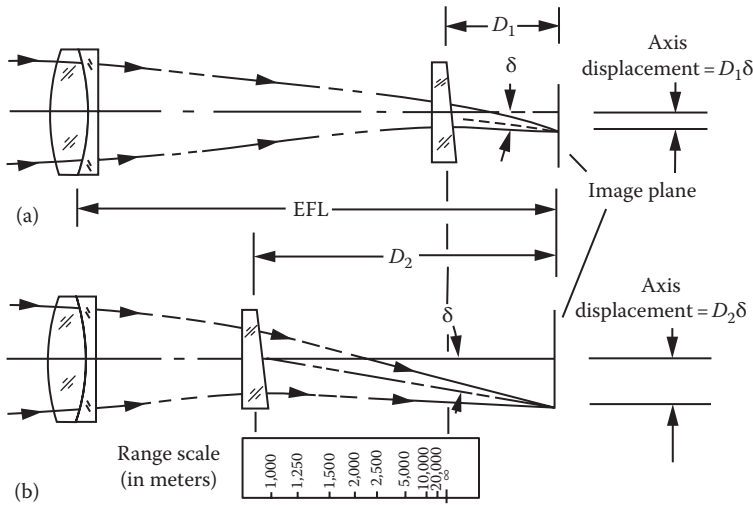
The function of a Risley wedge prism system: (a) bases together with deviation down, (b) bases opposed for zero deviation, (c) bases together for deviation up, and (d) general case with wedges counterrotated by $\pm\beta$. (From Yoder, PR., Jr., *Mounting Optics in Optical Instruments*, 2nd edn., SPIE Press, Bellingham, WA, 2008.)

Another arrangement has a single Risley wedge system mounted such that both wedges can be rotated together about the optical axis as well as counter rotated with respect to each other. This provides variation of deviation in a polar coordinate system.

7.6.6.3 Image-Deviating Sliding Wedge

A wedge prism located in a converging beam will deviate the beam so that the image is displaced laterally by an amount proportional to both the wedge deviation (in radians) and the distance from the wedge to the image plane (see Figure 7.52 for a schematic of the device). If the prism is moved axially by $D_2 - D_1$, the image displacement varies from $D_1\delta$ to $D_2\delta$.

An important application for this device was in military optical range finders before the advent of the laser range finder. In the figure, a range scale shows the change in range to a target as a function of wedge movement for one arm of a typical range finder, such as that shown

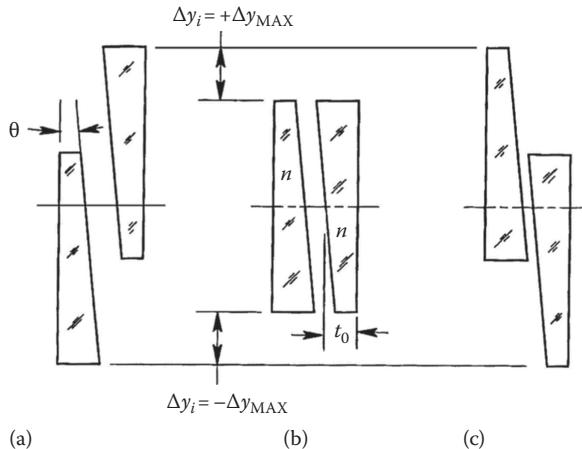
**FIGURE 7.52**

Axially sliding wedge beam deviating system for an optical range finder. View (a) applies to a distant target, while view (b) applies to a nearby one. (Adapted from Kaspereit, O.K., *Design of Fire Control Optics ORDM 2-1*, Vol. I, U.S. Army, Washington, DC, 1953.)

in Figure 7.51. Note that this is a nonlinear variation. This principle can be used in other more contemporary applications in which an image needs to be variably displaced laterally by a small distance. If used with a long focal-length lens, the wedge should be achromatic.

7.6.6.4 Focus-Adjusting Wedge System

Two identical optical wedges arranged with their bases opposite and mounted in linear stages so that each can be translated laterally by equal amounts relative to the optical axis

**FIGURE 7.53**

A focus-adjusting wedge system: (a) minimum optical path, (b) nominal optical path, and (c) maximum optical path. (From Yoder, P.R., Jr, *Mounting Optics in Optical Instruments*, 2nd edn., SPIE Press, Bellingham, WA, 2008.)

provide a variable optical path through glass. Figure 7.53 shows the principle of operation of the device. At all settings, the two wedges act as a plane-parallel plate. If located in a convergent beam, this system allows the image distance to be varied and can be used to bring images of objects at different distances into focus at a fixed image plane.

This type of focus-adjusting system has been used in large aperture aerial cameras and telescopes such as those used for tracking missiles or spacecraft launch vehicles where target range changes rapidly and the image-forming optics are large and heavy so they cannot be moved rapidly and precisely to maintain focus. To a first-order approximation, $t_1 = t_0 \pm \Delta y_i \tan \theta$ and the focus variation is $2t_i[(n - 1)/n]$. Here, t_0 is the axial thickness of each wedge at its geometric center.

Figure 7.54 shows the optical schematic for a typical application featuring a focus-adjusting wedge system. The system is the recording optical tracking instrument (ROTI) used to track early spacecraft launches at Cape Canaveral and other sites. As described in MIL-HDBK-141 (1962), it is basically an $f/4.17$ Newtonian telescope with a series of collimating doublet lenses and five Biotar-type photographic objectives forming a five-step selectable variable magnification lens subsystem following the tracking reticle located at primary mirror focus. The minimum EFL of the system is 100 in. (2.54 m). This is variable in equal steps to 500 in. (12.7 m).

The focus wedges immediately in front of the reticle in this telescope changed the glass path as the wedges were moved laterally so as to vary system focus in object space from infinity to ~ 2750 m. The wedge mechanism was linked to a radar system that measured range in real time to keep the photographic system in focus. Two operators controlled the line of sight of the system by observing the target through two auxiliary elbow telescopes, one for azimuth and the other for elevation. Both of these telescopes were attached to the main telescope mount and boresighted to the latter instrument.

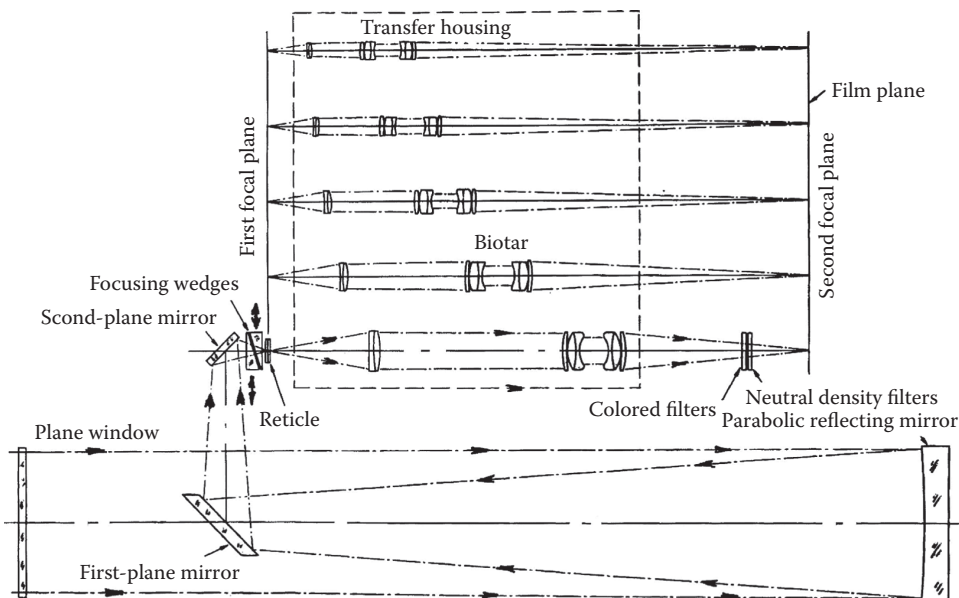


FIGURE 7.54

Optical schematic of the ROTI featuring an adjustable wedge focusing system. (From MIL-HDBK-141, *Optical Design*, Defense Supply Agency, Washington, DC, 1962.)

7.7 Anamorphic Prism Systems

A refracting prism used at other than minimum deviation changes the width of a transmitted collimated beam in the plane of refraction (see Figure 7.55a). The beam width in the orthogonal plane (perpendicular to the plane of the figure) is unchanged, so anamorphic magnification results. The beam is deviated by the prism and chromatic aberration is introduced. Both of these defects can be eliminated if two identical prisms are arranged in opposition as shown in Figure 7.55b. Lateral displacement of the axis then occurs, but the angular deviation and chromatic aberration are zero. The beam compression or expansion ratio depends upon the prism apex angles, the refractive indices, and the orientations of the two prisms relative to the input axis. The configuration shown in Figure 7.55b is a telescope in one meridian because the degree of collimation of the beam is unchanged while it is passing through the optics.

Two-prism anamorphic telescopes were first described by Brewster in about 1835 to replace the cylindrical lenses then used for the purpose (Kingslake, 1983). They are commonly used today to change diode laser beam size and angular divergence differentially in orthogonal directions or to convert rectangular laser beams, such as those from excimer lasers, into more suitably shaped square ones for materials processing and surgical applications (L'Esperance et al., 1989). The telescope shown in Figure 7.56a has achromatic prisms to allow a broad spectral range to be covered (Lohmann and Stork, 1989). Anamorphic telescopes with many cascaded prisms to produce higher magnification have been described. An extreme example with 10 prisms is shown in Figure 7.56b. This configuration is reported to be optimal for single-material achromatic expanders of moderate to large magnifications (see Trebino, 1985; Trebino et al., 1985).

An interesting anamorphic telescope consisting of only one prism from Forkner (1986) is shown in Figure 7.56c. It has three active faces, one of which reflects by TIR. The entrance and exit faces can be oriented at Brewster's angle so the Fresnel reflection losses at those surfaces are eliminated for polarized beams.

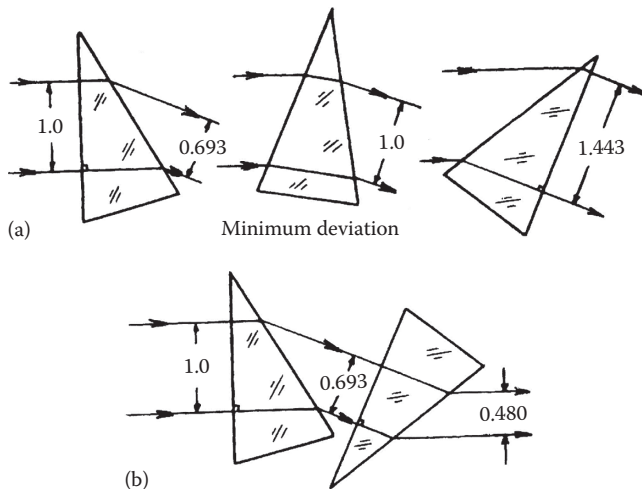
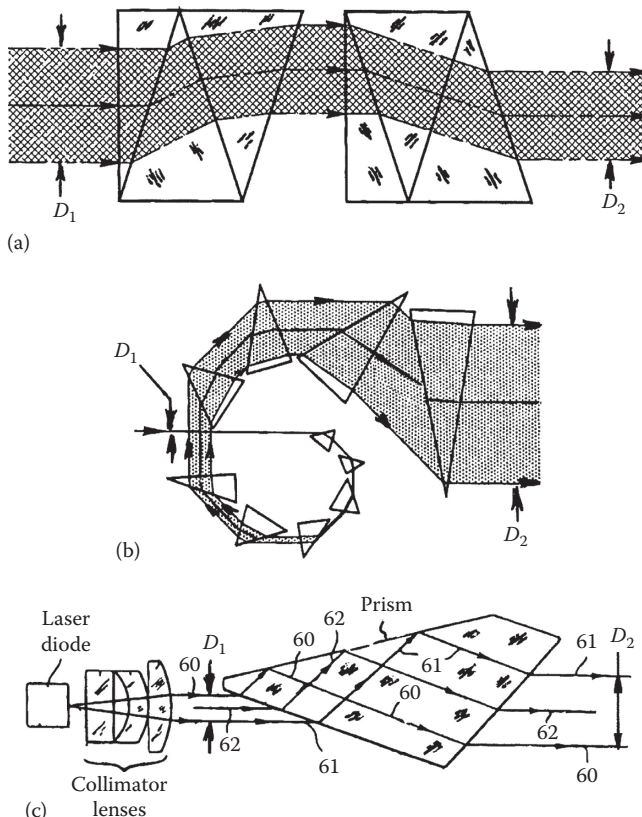


FIGURE 7.55

Functions of anamorphic prisms: (a) individual prisms at various incident angles and (b) an anamorphic telescope. (Adapted from Kingslake, R., *Optical System Design*, Academic Press, Orlando, FL, 1983.)

**FIGURE 7.56**

Three anamorphic prism telescope optical systems. (a) An achromatic prism assembly. (Adapted from Lohmann, A.W. and Stork, W., *Appl. Opt.*, 28, 1318, 1989.) (b) A cascaded anamorphic system. (Adapted from Trebino, R., *Appl. Opt.*, 24, 1130, 1985.) (c) A single-prism anamorphic prism for beam shaping. (Adapted from Forkner, J.F., US Patent No. 4,623,225, 1986.)

References

- De Vany, A.S., *Master Optical Techniques*, Wiley, New York, 1981.
 Forkner, J.F., Anamorphic prism for beam shaping, US Patent No. 4,623,225, 1986.
 Hopkins, R.E., Mirror and prism systems, in *Applied Optics and Optical Engineering*, Kingslake, R., Ed., Vol. III, Academic Press, New York, 1965, Chapter 7.
 Kaspereit, O.K., Ordnance Technical Notes No. 14, *Designing of Optical Systems for Telescopes*, U.S. Army, Washington, DC, 1933.
 Kaspereit, O.K., *Design of Fire Control Optics ORDM 2-1*, Vol. I, U.S. Army, Washington, DC, 1953.
 Kingslake, R., *Optical System Design*, Academic Press, Orlando, FL, 1983.
 L'Esperance, F.A., Jr., Warner, J.W., Telfair, W.B., Yoder, P.R., Jr., and Martin, C.A., Excimer laser instrumentation and technique for human corneal surgery, *Arch. Ophthalmol.*, 107, 131–139, 1989.
 Lohmann, A.W. and Stork, W., Modified Brewster telescopes, *Appl. Opt.*, 28, 1318, 1989.
 MIL-HDBK-141, *Optical Design*, Defense Supply Agency, Washington, DC, 1962.
 Patrick, F.B., Military optical instruments, in *Applied Optics and Optical Engineering*, Kingslake, R., Ed., Vol. V, Academic Press, New York, 1969, Chapter 7.

- Sar-El, H.Z., Revised Dove prism formulas, *Appl. Opt.*, 30, 30, 1991.
- Seil, K., Progress in binocular design, *Proc. SPIE*, 1533, 48, 1991.
- Seil, K., Private communication, 1997.
- Smith, W.J., *Modern Optical Engineering*, 4th edn., McGraw-Hill, New York, 2008.
- Trebino, R., Achromatic N-prism beam expanders: optimal configurations, *Appl. Opt.*, 24, 1130, 1985.
- Trebino, R., Barker, C.E., and Siegman, A.E., Achromatic N-prism beam expanders: Optimal configurations II, *Proc. SPIE*, 540, 104, 1985.
- Walles, S. and Hopkins, R.E., The orientation of the image formed by a series of plane mirrors, *Appl. Opt.*, 3, 1447, 1964.
- Wolfe, W.L., Nondispersing prisms, in *OSA Handbook of Optics*, 2nd edn., Bass, M., Van Stryland, E., Williams, D.R., and Wolfe, W.L., Eds., Vol. II, McGraw-Hill, New York, 1995, Chapter 4.
- Yoder, P.R., Jr., Study of light deviation errors in triple mirrors and tetrahedral prisms, *J. Opt. Soc. Am.*, 48, 496, 1958.
- Yoder, P.R., Jr., Two new lightweight military binoculars, *J. Opt. Soc. Am.*, 50, 491, 1960.
- Yoder, P.R., Jr., *Mounting Optics in Optical Instruments*, 2nd edn., SPIE Press, Bellingham, WA, 2008.
- Yoder, P.R., Jr., Schlesinger, E.R., and Chickvany, J.L., Active annular-beam laser autocollimator, *Appl. Opt.*, 14, 1890, 1975.
- Yoder, P.R., Jr. and Vukobratovich, D., *Field Guide for Binoculars and Scopes*, SPIE Press, Bellingham, WA, 2011.